

Spatiotemporal prediction of wildfire extremes with Bayesian finite sample maxima

Maxwell B. Joseph^{*1}, Matthew W. Rossi¹, Nathan P. Mietkiewicz¹, Adam L. Mahood¹,
Megan E. Cattau¹, Lise Ann St. Denis¹, R. Chelsea Nagy¹, Virginia Iglesias¹, John T.
Abatzoglou², and Jennifer K. Balch¹

¹Earth Lab, University of Colorado Boulder

²Department of Geography, University of Idaho

Abstract

Wildfires are becoming more frequent in parts of the globe, but predicting where and when wildfires occur remains difficult. To predict wildfire extremes across the contiguous United States, we integrate a 30 year wildfire record with meteorological and housing data in spatiotemporal Bayesian statistical models with spatially varying nonlinear effects. We compared different distributions for the number and sizes of large fires to generate a posterior predictive distribution based on finite sample maxima for extreme events (the largest fires over bounded spatiotemporal domains). A zero-inflated negative binomial model for fire counts and a lognormal model for burned areas provided the best performance. This model attains 99% interval coverage for the number of fires and 93% coverage for fire sizes over a six year withheld data set. Dryness and air temperature strongly predict extreme wildfire probabilities. Housing density has a hump-shaped relationship with fire occurrence, with more fires occurring at intermediate housing densities. Statistically, these drivers affect the chance of an extreme wildfire in two ways: by altering fire size distributions, and by altering fire frequency, which influences sampling from the tails of fire size distributions. We conclude that recent extremes should not be surprising, and that the contiguous United States may be on the verge of even larger wildfire extremes.

*maxwell.b.joseph@colorado.edu

Key words: fire; wildfire; Bayesian; spatiotemporal; extremes; climate.

1 Introduction

2 Wildfire frequency and burned area has increased over the past couple decades in the
3 United States (Dennison et al. 2014; Westerling 2016), and elsewhere (Krawchuk et al.
4 2009; Pechony and Shindell 2010). In addition to the ecological and smoke impacts associ-
5 ated with increased burned area, there has been an increasing interest in extreme wildfires
6 (Williams 2013) given their impact on human lives and infrastructure (Kochi et al. 2010;
7 Diaz 2012). While case studies of particular extremes provide insight into what caused
8 past events (Peterson et al. 2015; Nauslar, Abatzoglou, and Marsh 2018), predictions of
9 future extremes at a national level could inform disaster related resource allocation. The
10 term “extreme” has multiple meanings with respect to wildfires (Tedim et al. 2018), and
11 in this paper we take consider an extreme wildfire to be a fire with the largest burned area
12 over a bounded spatiotemporal domain, i.e., the block maximum within a spatial region
13 and a temporal interval (Coles et al. 2001). For example, the block maxima for wildfires
14 across the contiguous U.S. can be defined on a yearly basis (Figure 1).

15 Factors driving wildfire extremes vary in space and time (Barbero et al. 2014), but it is
16 unclear how best to account for this in a predictive model. Previous efforts have used year
17 or region-specific models, aggregating over space or time (Bermudez et al. 2009), tempo-
18 rally or spatially explicit models (Mendes et al. 2010), and spatial models with year as a
19 covariate (Díaz-Avalos, Juan, and Serra-Saurina 2016). Recently, rich spatiotemporal mod-
20 els have been described with linear, spatially constant covariate effects (Serra, Saez, Juan,
21 et al. 2014; Serra, Saez, Mateu, et al. 2014). However, linear, spatially constant effects
22 are suboptimal over large spatial domains with nonlinear drivers (Fosberg 1978, Goodrick
23 (2002), Preisler et al. (2004); Preisler and Westerling 2007; Balshi et al. 2009; Krawchuk et
24 al. 2009; Pechony and Shindell 2009; Vilar et al. 2010; Woolford et al. 2011; Woolford et
25 al. 2014). For example, global wildfire probability shows a hump-shaped relationship with
26 temperature and moisture (Moritz et al. 2012). Interactions among drivers also impose

27 nonlinearity, e.g., in hot and dry climates fires are fuel limited (McLaughlin and Bowers
28 1982), but in cold and wet climates fires are energy limited (Krawchuk and Moritz 2011).
29 Prediction is also complicated by uncertainty in which distribution(s) to use to assign
30 probabilities to extreme events. The generalized Pareto distribution (GPD) has frequently
31 been used (Bermudez et al. 2009; Jiang and Zhuang 2011), but the GPD requires a thresh-
32 old to delineate extreme events (Davison and Smith 1990, Coles (2014)). The utility and
33 validity of a threshold for extremes in a heterogeneous region is debatable (Tedim et al.
34 2018). Recently proposed metastatistical extreme value (MEV) approaches do not require
35 such a threshold, and are based on the statistical distribution of finite sample maxima, i.e.,
36 the probability distribution of the maximum value for a finite number of events (Marani
37 and Ignaccolo 2015; Zorzetto, Botter, and Marani 2016). In the MEV framework, the oc-
38 currence and size of future events, and the parameters of their distributions are treated
39 as random variables which together imply a distribution for extremes. This approach has
40 roots in compound distributions (Dubey 1970; Wiitala 1999), doubly stochastic processes
41 (Cox and Isham 1980), superstatistics (Beck and Cohen 2003), and the Bayesian posterior
42 predictive distribution (Gelman et al. 2013). The link to Bayesian inference is particularly
43 useful, as it provides an easy way to propagate uncertainty forward to to predictions of
44 extremes (Coles, Pericchi, and Sisson 2003).

45 Here, we extend the finite sample maximum approach to account for non-linear, spatially
46 varying covariate effects with the goal of predicting extreme wildfire events from a sta-
47 tistical perspective across the contiguous United States. Specifically, we aim to predict
48 occurrence (where and when), and magnitude (burned area) of large wildfires at a monthly
49 time scale and regional spatial scale across the contiguous United States.

50 **Methods**

51 **Data description**

52 We acquired wildfire event data for the contiguous United States from the Monitoring
53 Trends in Burn Severity (MTBS, www.mtbs.gov) program (Eidenshink et al. 2007), which
54 includes spatiotemporal information on the occurrence of wildfires in the United States
55 from 1984 to 2016. The MTBS data contain fires greater than 1000 acres (\approx 405 hectares)
56 in the western U.S. and greater than 500 acres (\approx 202 hectares) in the eastern U.S. For
57 consistency across the U.S., we discarded all records in the MTBS data less than 1000
58 acres, retaining 10,736 fire events (Figure 2A). Each event in the MTBS data has a discov-
59 ery date, spatial point location, and final size.

60 To explain fire size and occurrence, we used a combination of meteorological variables in-
61 cluding humidity, air temperature, precipitation, and wind speed. These variables were
62 selected on the basis of previous work, and also with an aim to drive a predictive model
63 with interpretable meteorological quantities. Meteorological layers were acquired from the
64 gridMET data (Abatzoglou 2013) that blends monthly high-spatial resolution (\sim 4-km)
65 climate data from the Parameter-elevation Relationships on Independent Slopes Model
66 (Daly et al. 2008) with high-temporal resolution (hourly) data from the National Land
67 Data Assimilation System (NLDAS2) using climatologically aided interpolation. The resul-
68 tant products are a suite of surface meteorological variables summarized at the daily time
69 step and at a 4-km pixel resolution. Daily total precipitation, minimum relative humidity,
70 mean wind speed, and maximum air temperature were averaged at a monthly time step for
71 each of 84 Environmental Protection Agency level 3 (L3) ecoregions for each month from
72 1984 to 2016 (Omernik 1987; Omernik and Griffith 2014). We also computed cumulative
73 monthly precipitation over the previous 12 months for each ecoregion-month combina-
74 tion. We chose to segment the U.S. with level 3 ecoregions as a compromise between the
75 more numerous (computationally demanding) level 4 ecoregions, and the coarser level 2
76 ecoregions.

77 We used publicly available housing density estimates that were generated based on the
78 U.S. 2000 decennial census as explanatory variables that may relate to human ignition
79 pressure (Radeloff et al. 2010). These are provided at decadal time steps, and spatially
80 at the level of census partial block groups. To generate approximate measures of hous-
81 ing density at monthly time intervals, we used a simple linear interpolation over time for
82 each block group, then aggregated spatially across block groups to compute mean housing
83 density for each ecoregion in each month.

84 **Model development**

85 We built two types of models: one describing the occurrence of fires within each L3 ecore-
86 gion over time (i.e., the total number of fires occurring in each ecoregion for each month
87 from 1984 - 2016), and another describing the size of each wildfire in each ecoregion and
88 month. For occurrence models, the response variable was a count (number of fires), and
89 for burned area models, the response was a continuous positive quantity (size of each fire
90 event). We used the period from 1984 to 2009 for training, withholding the period from
91 2010 to 2016 to evaluate predictive performance.

92 **Fire occurrence**

93 We constructed four models for fire occurrence and compared their predictive performance
94 based on test-set log likelihood and posterior predictive checks for the proportion of zeros,
95 maximum count, and total count. The models differed in the distributions used in the like-
96 lihood, representing counts as a Poisson, negative binomial, zero-inflated Poisson, or zero-
97 inflated negative binomial random variable. The Poisson distribution is a common choice
98 for counts, and the negative binomial distribution provides an alternative that can account
99 for overdispersion. The zero-inflated versions of these distributions include a component
100 to represent extra zeros, which might be expected to work well if there are independent
101 processes that determine whether nonzero counts are possible (Lambert 1992).

102 For spatial units (ecoregions) $s = 1, \dots, S$ and time steps (months) $t = 1, \dots, T$, each

103 model defines a probability mass function for $n_{s,t}$: the number of fires over 405 hectares in
104 ecoregion s and time step t . For each of the four count distributions under consideration,
105 location parameters $\mu_{s,t}$ and (for zero-inflated models) structural zero inflation parameters
106 $\pi_{s,t}$ were allowed to vary in space and time. We used a log link function to ensure that
107 $\mu_{s,t} > 0$, and a logit link function to ensure that $\pi_{s,t} \in (0, 1)$. Concatenating over spatial
108 and temporal units, so that $\boldsymbol{\mu} = (\mu_{s=1,t=1}, \mu_{s=2,t=1}, \dots, \mu_{s=S,t=1}, \mu_{s=S,t=2}, \dots, \mu_{s=S,t=T})$, and
109 similarly for $\boldsymbol{\pi}$, we modeled location and (when applicable) zero inflation parameters as:

$$\log(\boldsymbol{\mu}) = \alpha^{(\mu)} + \mathbf{X}\boldsymbol{\beta}^{(\mu)} + \boldsymbol{\phi}^{(\mu)} + \log(\mathbf{a}),$$

$$\text{logit}(\boldsymbol{\pi}) = \alpha^{(\pi)} + \mathbf{X}\boldsymbol{\beta}^{(\pi)} + \boldsymbol{\phi}^{(\pi)},$$

110 where $\alpha^{(\mu)}$ and $\alpha^{(\pi)}$ are scalar intercept parameters, \mathbf{X} is a known $(S \times T) \times p$ design matrix,
111 where p is the number of input features, $\boldsymbol{\beta}^{(\mu)}$ and $\boldsymbol{\beta}^{(\pi)}$ are column vector parameters of
112 length p , $\boldsymbol{\phi}^{(\mu)}$ and $\boldsymbol{\phi}^{(\pi)}$ are column vector parameters of length $S \times T$ containing spatiotem-
113 poral adjustments, and \mathbf{a} is a known offset vector of areas for spatial unit $s = 1, 2, \dots, S$,
114 repeated T times.

115 Burned area

116 We developed five candidate models for fire size, each of which specified a different distri-
117 bution for the size (burned area) of individual fire events (Reed and McKelvey 2002; Her-
118 nandez et al. 2015), including the generalized Pareto (Hosking and Wallis 1987), tapered
119 Pareto (Schoenberg, Peng, and Woods 2003), lognormal, gamma, and Weibull distribu-
120 tions. We evaluated each model in terms of test set log likelihood, and posterior predictive
121 checks for fire size extremes. We defined the response y_i as the number of hectares burned
122 over 405 for the i^{th} fire event, which occurred in spatial unit s_i and time step t_i .

123 Because each burned area distribution has a different parameterization, we included
124 covariate effects in a distribution-specific way. For the generalized Pareto distribution

125 (GPD), we assumed a positive shape parameter, leading to a Lomax distribution for ex-
126 ceedances (Bermudez et al. 2009). The GPD and Lomax shape parameters are related by
127 $\kappa^{(GPD)} = 1/\kappa^{(L)}$, and the GPD scale parameter is related to the Lomax scale and shape
128 parameters by $\sigma^{(GPD)} = \sigma^{(L)}/\kappa^{(L)}$. We introduced covariate dependence via the Lomax
129 scale parameter using a log link. For event i , $\log(\sigma_i^{(L)}) = \alpha + \mathbf{X}_{(s_i, t_i)}\boldsymbol{\beta} + \phi_{s_i, t_i}$, where α is
130 an intercept parameter, $\boldsymbol{\beta}$ is a length p vector of coefficients, $\mathbf{X}_{(s_i, t_i)}$ is a row vector from
131 \mathbf{X} , and ϕ_{s_i, t_i} is a spatiotemporal adjustment for s_i and t_i . For the tapered Pareto model,
132 we modeled the shape parameter as $\log(\kappa_i) = \alpha + \mathbf{X}_{(s_i, t_i)}\boldsymbol{\beta} + \phi_{s_i, t_i}$. The lognormal model
133 included covariate dependence via the location parameter: $\mu_i = \alpha + \mathbf{X}_{(s_i, t_i)}\boldsymbol{\beta} + \phi_{s_i, t_i}$. The
134 gamma model used a log link for the expected value: $\log(E(y_i)) = \alpha + \mathbf{X}_{(s_i, t_i)}\boldsymbol{\beta} + \phi_{s_i, t_i}$. Last,
135 we modeled the Weibull scale parameter as $\log(\sigma_i) = \alpha + \mathbf{X}_{(s_i, t_i)}\boldsymbol{\beta} + \phi_{s_i, t_i}$. More detail on
136 the parameterization of each burned area distribution is provided in the Appendices.

137 **Accounting for nonlinear forcing**

138 The design matrix \mathbf{X} was constructed to allow for spatially varying nonlinear effects of
139 housing density and meteorological drivers. We used B-splines to account for nonlinearity
140 (Figure 3) and allowed the coefficients for each basis vector to vary spatially (Wood 2017).
141 First, we constructed univariate B-splines for log housing density, wind speed, same month
142 precipitation, previous 12 month precipitation, air temperature, and humidity, with five
143 degrees of freedom (including an intercept) for each variable. This step generated 30 basis
144 vectors (five for each of six variables).

145 To allow for spatial variation in these nonlinear effects, we added interaction effects be-
146 tween each of the basis vectors and ecoregions (Brezger and Lang 2006; Kneib, Hothorn,
147 and Tutz 2009). The hierarchical nesting of ecoregion designations (Figure 2B-D) lends
148 itself to such interactions. Conceptually, coefficients in a level 3 ecoregion may be related
149 to coefficients in the level 2 ecoregion containing the level 3 region, the level 1 ecoregion
150 containing the level 2 region, and a global effect. The coefficient associated with a basis
151 vector for any level 3 ecoregion is treated as a sum of a global effect, a level 1 ecoregion
152 adjustment, a level 2 ecoregion adjustment, and a level 3 ecoregion adjustment. Thus,

153 for every univariate basis vector, we included interaction effects with ecoregion at each of
154 the three ecoregion levels. This allows borrowing of information across space (level 3 ecore-
155 gions in a level 2 ecoregion are often adjacent), and for regions that are ecologically similar.
156 We also included adjustments on the global intercept for each level 1, 2, and 3 ecoregion to
157 account for spatial variation that is unrelated to climate or housing density. This specifica-
158 tion induces sparsity in \mathbf{X} that we exploit to increase the efficiency of computing $\boldsymbol{\mu}$ and $\boldsymbol{\pi}$.
159 In total, \mathbf{X} has $p = 3,472$ columns, with 97% zero entries.

160 **Prior specification**

161 To avoid overfitting, we used a regularized horseshoe prior on the coefficients associated
162 with the spatially varying nonlinear effects described above (Piironen, Vehtari, and others
163 2017). This prior places high probability close to zero, while retaining heavy enough tails
164 that nonzero coefficients are not shrunk too strongly toward zero. This is consistent with
165 our prior expectation that most of the coefficients associated with the columns in \mathbf{X} were
166 close to zero. For the zero inflated count models, we used a multivariate horseshoe to allow
167 information sharing between the zero inflated and distribution specific location parameters
168 (Peltola et al. 2014). For the remaining count models and all burned area models, this
169 was a univariate horseshoe prior. Spatiotemporal random effects were constructed using
170 a temporally autoregressive, spatially intrinsically autoregressive formulation (Besag and
171 Kooperberg 1995; Banerjee, Carlin, and Gelfand 2014). Details of these priors and the
172 resulting joint distributions are provided in the Appendices.

173 **Posterior predictive inference for finite sample maxima**

174 We used the posterior predictive distribution to check each model and make inference on
175 extremes. The posterior predictive distribution provides a distribution for replications
176 of observed data (y^{rep}), and predictions of future data (Gelman et al. 2013). Concep-
177 tually, for a good model, y^{rep} should be similar to observed training data y , and future
178 predictions should be similar to future data. Distributions over both quantities can be

179 obtained by conditioning on y and marginalizing over model parameters θ , e.g., $[y^{\text{rep}}|y] =$
180 $\int [y^{\text{rep}}|\theta][\theta|y]d\theta$.

181 Posterior predictive distributions facilitate model checks that compare predicted and ob-
182 served test statistics (Gelman, Meng, and Stern 1996). To evaluate whether models cap-
183 tured tail behavior, we compared empirical maxima ($T(y) = \max(y)$) to the predicted
184 distribution of maxima $T(y^{\text{rep}})$. We also include predictive checks for the proportion of
185 zero counts, and totals for count and burned area models. Posterior predictive inference
186 for finite sample maxima is similar in spirit to the MEV approach. Both obtain a distri-
187 bution over maxima by marginalizing over unknowns including the number of events, size
188 of each event, and parameters of their distributions (Marani and Ignaccolo 2015). How-
189 ever, a Bayesian approach explicitly conditions on the observed data to obtain a posterior
190 distribution of parameters.

191 Seeing this connection is useful in the context of including priors and propagating uncer-
192 tainty to derived parameters. For any ecoregion s and timestep t , if we define a particular
193 maximum fire size conditional on a fire having occurred as $z_{s,t}$, and let $Z_{s,t}$ represent the
194 random variable of maximum fire size, then the cumulative distribution function (CDF)
195 for $z_{s,t}$ is given by $\Pr(Z_{s,t} \leq z_{s,t}) = F(y_{(s,t)})^{n_{s,t}}$, where $F(y_{(s,t)})$ is the CDF of fire size, and
196 $n_{s,t}$ is the number of wildfire events. Thus, $\Pr(Z_{s,t} \leq z_{s,t})$ is the distribution function for
197 the finite sample maximum. The CDF for $z_{s,t}$ can be inverted to produce a quantile func-
198 tion that permits computation of prediction intervals for maximum fire sizes, conditional
199 on fires having occurred. Given a collection of posterior draws from a burned area model
200 that parameterize $F(y_{(s,t)})$, and a collection of posterior draws of $n_{s,t}^{\text{rep}}$ from the posterior
201 predictive distribution of a wildfire count model, a posterior distribution for the CDF or
202 quantile function of maximum fire size can be generated which combines the two models
203 to facilitate inference on the distribution of extremes.

204 **Parameter estimation**

205 We used a combination of variational approximations and Hamiltonian Monte Carlo meth-
206 ods to sample from the posterior distributions of count and burned area models. A varia-
207 tional approximation (Kucukelbir et al. 2015) was used for count models to quickly iden-
208 tify a preferred model. The best performing count model and all burned area models were
209 fit using the No-U-Turn Sampler (Hoffman and Gelman 2014). Models were fit in the Stan
210 probabilistic programming language using the `rstan` package (Carpenter et al. 2016; Stan
211 Development Team 2018). We ran four chains for 1000 iterations each, discarding the first
212 500 iterations as warmup. Convergence was assessed using visual inspection of trace plots,
213 with potential scale reduction statistic values $\hat{R} \geq 1.1$ as an indicator convergence failure
214 (Brooks and Gelman 1998).

215 **Implementation**

216 All data processing, model fitting, and visualization were implemented with open source
217 software, primarily in the R programming language (R Core Team 2017), and wrapped in
218 a reproducible workflow via GNU Make and Docker (Stallman, McGrath, and Smith 2004;
219 Boettiger 2015). Data cleaning and transformation required the R packages `assertthat`
220 (Wickham 2017a), `lubridate` (Grolemund and Wickham 2011), `Matrix` (Bates and Maech-
221 ler 2018), `pbapply` (Solymos and Zawadzki 2018), `splines` (R Core Team 2018), `tidyverse`
222 (Wickham 2017b), and `zoo` (Zeileis and Grothendieck 2005). Spatial data were processed
223 with `raster` (Hijmans 2017), `rgdal` (Bivand, Keitt, and Rowlingson 2018), `sf` (Pebesma
224 2018), and `spdep` (Bivand and Piras 2015). Finally, we used `cowplot` (Wilke 2017), `ggre-`
225 `pel` (Slowikowski 2018), `ggthemes` (Arnold 2018), `patchwork` (Pedersen 2017), and `RCol-`
226 `orBrewer` (Neuwirth 2014) for visualization. The manuscript was written in R Mark-
227 down (Allaire et al. 2018). Analyses were run on an Amazon Web Services m5.2xlarge
228 EC2 instance with four physical cores and 32 GB of RAM, and the whole workflow re-
229 quires ≈ 72 hours. All code to reproduce the analysis is available on GitHub at <https://github.com/mbjoseph/wildfire-extremes> (Joseph 2018).
230

231 Results

232 Wildfire occurrence

233 The zero-inflated negative binomial distribution performed best on the held-out test set
234 (Table 1), and was able to recover the proportion of zeros, count maxima, and count to-
235 tals in posterior predictive checks for both the training and test data (Figure 4). All of
236 the other count models that we considered exhibited lack of fit to at least one of these
237 statistics in posterior predictive checks. Hereafter, we report results from the zero-inflated
238 negative binomial model.

239 Minimum relative humidity and maximum air temperature had the strongest effects on
240 both the zero-inflation component and the expected value of the negative binomial com-
241 ponent (Figure 5, posterior median for ρ : 0.665, 95% credible interval (CI): 0.319 - 0.861).
242 The model uncovered unique effects of meteorological variables at level 1, 2, and 3 ecore-
243 gions (Figure 6). For example, a positive interaction effect between the second air temper-
244 ature basis vector and the L1 Great Plains ecoregions indicates that the expected number
245 of wildfires in plains ecoregions with cold conditions is high relative to other ecoregions.
246 The Ozark/Ouachita-Appalachian forest and Ozark Highlands were also identified as
247 having region-specific temperature effects (Figure 6). Twelve month total precipitation
248 also had region specific effects in the Mississippi Alluvial and Southeast Coastal Plains
249 ecoregion, where it was associated with lower expected fire counts (Figure 6). In contrast,
250 increasing cumulative twelve month precipitation was associated with higher counts in
251 desert ecoregions (Figure 5). Housing density showed a unimodal relationship to expected
252 count (Figure 5), with lower expected counts in sparsely populated ecoregions, and higher
253 expected counts with moderately populated ecoregions.

254 Posterior 95% credible interval coverage for the number of fires over 405 hectares in the
255 test set was 98.8%. The lowest test set interval coverage was 89.3%, in the Cross Timbers
256 L3 ecoregion. When observed counts fell outside the 95% prediction interval, counts were
257 larger than predicted 100% of the time. The largest difference between observed numbers

258 and predicted 97.5% posterior quantiles (the upper limit for the 95% credible interval) oc-
259 curred for the Columbia Mountains/Northern Rockies L3 ecoregion in August 2015, when
260 36 fires over 405 hectares occurred and at most 22 were predicted. For nearly half of the
261 level 3 ecoregions (43 of 85), accounting for 39.7% of the land area of the contiguous U.S.,
262 the zero-inflated negative binomial model had 100% test set prediction interval coverage.

263 **Wildfire burned areas**

264 The lognormal distribution performed best on the test set (Table 2), and captured tail-
265 behavior better than other burned area distributions (Figure 7). The GPD model was too
266 heavy-tailed to adequately capture the pattern in the empirical data, predicting fires far
267 larger than those observed in the training and test sets (Figure 7). The tapered Pareto
268 distribution was too light-tailed (Figure 7). The gamma and Weibull models performed
269 very poorly overall on the test set (Table 2), apparently due to a lack of congruence be-
270 tween the shapes of these distributions and the actual burned area distribution. Despite
271 a poor fit to the bulk of the wildfire burned area distribution, both performed adequately
272 in the upper tails (Figure 7). Hereafter we present results for the lognormal model, which
273 had the highest test set log likelihood and captured tail behavior of the empirical fire size
274 distribution.

275 Relative humidity was the primary driver of expected burned area for a fire event (Figure
276 8A). The first basis vector for mean daily minimum relative humidity was the only coeffi-
277 cient with a 95% credible interval that did not include zero (posterior median: 1.68, 95%
278 CI: (0.8 - 2.29)). This nonlinear effect can be observed in Figure 8B as an increase in the
279 expected burned area below 20% mean daily minimum humidity. This leads to a season-
280 ality gradient among ecoregions of expected fire sizes, with little or no seasonal signal in
281 typically humid ecoregions such as Marine West Coast Forests of the Pacific Northwest,
282 and seasonal oscillations in ecoregions that have periodic fluctuations between dry and hu-
283 mid conditions such as the Temperate Sierras (Figure 8C). There was not strong evidence
284 that meteorological variables had spatially variable effects on expected wildfire burned
285 area.

286 Overall, 95% posterior predictive interval coverage in the test set for burned areas was
287 93%. The lowest test set coverage was 0%, for the Eastern Great Lakes Lowlands L3 ecore-
288 gion, followed by 50%, for the Central California Valley L3 ecoregion, though these ecore-
289 gions had just 1 and 2 wildfire events in the test set. When observed fire sizes fell outside
290 the 95% prediction interval, 24.9% of wildfires were smaller than predicted, and 75.1% of
291 wildfires were larger than predicted. The largest discrepancy between the actual size of a
292 wildfire and the predicted 97.5% posterior quantile was observed with the Wallow Fire in
293 2011 which burned 228,107 hectares, but the predicted upper limit for size was 20,756. We
294 investigate this discrepancy further in the case study below. The lognormal burned area
295 model achieved 100% interval coverage in 24 of 67 ecoregions that had wildfire events in
296 the test set, accounting for 26% of the land area of the contiguous U.S.

297 **Inference on extremes**

298 By combining the output of the event count and burned area models, we derived pos-
299 terior prediction intervals for the size of the largest fire in a month for each region (the
300 “burned area maximum”), integrating over uncertainty in the number of fires, as well as
301 the lognormal mean and standard deviation for burned area. We evaluated the posterior
302 distribution for the quantile function of the finite sample maximum of a lognormal distri-
303 bution ($\exp(\mu + \sigma\sqrt{2}\text{erf}^{-1}(2P^{1/n} - 1))$), where n is the number of wildfire events, erf^{-1} is
304 the inverse error function, and P is a probability) to generate prediction intervals for maxi-
305 mum fire sizes by month and ecoregion, conditional on one or more fires having occurred.
306 In the holdout period from 2010 to 2016, a 99% prediction interval achieved 77.4% interval
307 coverage, with 14.8% of the burned area maxima (140 fire events) being larger than pre-
308 dicted (Figure 9). As an additional check, we used the posterior distribution of the model
309 to predict the total area burned by wildfires in the test set. The model predicted the total
310 area burned over the entire contiguous United States in test period from 2010 to 2016 to
311 be 30,339,123 (95% CI: (20,496,551 - 50,446,932) and the actual value was 30,440,173.

312 While fires over a million acres ($\approx 404,686$ hectares) in size have happened historically in
313 the contiguous U.S. (Pernin 1971), no such fires were represented in in the training or test

314 sets. If we extrapolate, the probability of at least one fire this large in the period from
315 2010 to 2016 was estimated to be between 0.191 and 0.651 (95% CI), with a posterior
316 median of 0.348. The highest probability for such an event was 0.014 (posterior median),
317 with a 95% CI of (0, 0.237) seen for the Southwestern Tablelands ecoregion in June 2011.
318 The second highest probability was 0.004 (posterior median), with a 95% CI of (0, 0.056)
319 seen for the Arizona/New Mexico Mountains ecoregion in June 2011. Aggregating spa-
320 tially, we estimated monthly probabilities of a million acre wildfire. These probabilities
321 show seasonal signals corresponding to peak fire seasons, with a shift toward higher and
322 broader peaks beginning in the 21st century (Figure 10).

323 **Error analysis case study: the 2011 Wallow Fire**

324 To better understand how well the model could or could not anticipate notable extreme
325 events, and why, we used the largest fire in the test set as a case study. The Wallow Fire
326 was accidentally ignited on May 29, 2011 by two campers in the L3 Arizona/New Mex-
327 ico Mountains ecoregion. It burned through the month of June and into early July. The
328 model underpredicted the total burned area of the Wallow Fire. Integrating over uncer-
329 tainty in the predicted number of fires and expected fire size, the 99% credible interval for
330 the maximum fire size for May 2011 was (730 - 107,419) hectares, but the Wallow Fire is
331 recorded as 228,103 hectares.

332 We evaluated the contribution of each covariate to the linear predictor functions of the
333 three model components (lognormal mean for burned areas, negative binomial mean for
334 counts, and the logit probability of the zero-inflation component) to understand why these
335 predictions differed. We defined the contribution of a variable as the dot product of the
336 elements in the design matrix \mathbf{X} corresponding to a particular driver variable (e.g., humid-
337 ity), and the estimated coefficients in β corresponding to that variable. This provides a
338 quantitative measure of how each input variable contributes to the linear predictor for an
339 ecoregion, and incorporates the overall, level 1, level 2, and level 3 ecoregion adjustments
340 on these effects. Humidity is the primary driver of variation in the model's predictions
341 overall, and June 2011 - the month after ignition - favored more large fires, with drier, hot-

342 ter conditions (Figure 11). The 99% credible interval for June 2011 was (4,258 - 428,765)
343 hectares, which contains the true value. Had the Wallow Fire ignited two days later, the
344 true final size would have been contained in the prediction interval. Evidently, conditions
345 in May that drove (under)predictions of maximum burned area were not representative of
346 the conditions over most of the Wallow Fire's duration.

347 Temporal mismatch aside, meteorological conditions local to the Wallow Fire differed
348 from the monthly regional means (Figure 12). In particular, wind speeds in the Wallow
349 Fire vicinity exceeded the regional monthly mean values on the date of ignition and in
350 the weeks following ignition. Over the majority of the duration of the Wallow Fire (May
351 29 to July 8), local daily conditions were drier and hotter on average than regional mean
352 monthly conditions in May, which were used to drive the statistical model. This local vari-
353 ability is not represented in the regional models developed here. The failure of the model
354 to correctly predict the size of the Wallow fire suggests potential avenues for improvement,
355 discussed below.

356 Discussion

357 Extreme wildfires are often devastating, but perhaps they need not be surprising. By
358 allowing the non-linear effects of weather and housing density to vary across space, this
359 model achieves good predictive accuracy for fire extremes at a regional scale over a six
360 year prediction window. This model predicts that extremely large wildfires, perhaps even
361 over one million acres (404,686 hectares), have a non-negligible probability of occurrence in
362 the contiguous United States. Such predictions can support regional wildfire management
363 and probabilistic hazard assessment.

364 Driving a model with meteorological features raises challenges related to predictive un-
365 certainty and covariate shift - a change in the underlying distribution of forcing variables,
366 potentially outside of the historic range. Ideally, this uncertainty would be propagated for-
367 ward in a predictive model, possibly through stacking of predictive distributions that are
368 generated from multiple models of future climate dynamics (Yao et al. 2017). But, even

369 if one had a perfect forecast, novel conditions present a challenge for predictive modeling
370 (Quionero-Candela et al. 2009). For example, the High Plains ecoregion had its highest
371 mean monthly precipitation, lowest 12 month running precipitation, driest, hottest, and
372 windiest conditions in the test set period. Extrapolating beyond the range of training in-
373 puts is generally difficult, but the hierarchical spatial effect specification used here allows
374 partial pooling among climatically similar ecoregions that can inform such predictions,
375 unlike models fit separately to disjoint spatial regions.

376 Similar issues could arise when making predictions for observed but rare meteorologi-
377 cal conditions. For example, mean daily minimum humidity values over 60% accounted
378 for just 3.76% of the ecoregion-months in the training data, and 0 fires occurred in such
379 months. As a consequence, there is relatively little data that can be used to inform the
380 model for such conditions, and the prior distribution which shrinks coefficients toward
381 zero may dominate the likelihood in the posterior distribution. In this case, the poste-
382 rior distribution for the last basis coefficient for the partial effect of humidity is likely to
383 be close to zero. This could explain why the estimated partial effect of humidity on the
384 expected counts was less negative at the upper end of the observed humidity range, al-
385 though previous work has found similarly nonlinear partial effects (Preisler et al. 2004).
386 The count model performed extremely well in this range, with 100% interval coverage for
387 the 299 ecoregion-months with mean daily minimum humidity values greater than 60%
388 in the withheld test data. The model nearly always predicted zero counts with high confi-
389 dence when conditions were this humid: 298 of 299 predictions made for such conditions
390 were 95% credible intervals of (0, 0). The remaining prediction had a posterior median of
391 zero, along with a 95% credible interval from 0 to 1. Monotonicity constraints could be
392 incorporated into these models via monotonic spline bases (Ramsay and others 1988), or
393 an ordered prior distribution for basis coefficients (Brezger and Steiner 2008). In this case,
394 the count model performs well under humid conditions without monotonicity constraints,
395 and there seems to be little room for performance improvements that might result from
396 such constraints.

397 Human-caused climate change is expected to increase fire activity in the western U.S.

398 (Rogers et al. 2011; Westerling et al. 2011; Moritz et al. 2012; Abatzoglou and Williams
399 2016) and elsewhere (Flannigan et al. 2009), but the nonlinear effect of housing density
400 could provide additional insight into future expectations. While housing density is increas-
401 ing over time in most U.S. ecoregions, some of these ecoregions are in the range of values
402 in which this increases the expected number of large fires, while others are so populated
403 that further increases would reduce the chance of a large fire. The hump-shaped effect of
404 human density on the expected number of large fires is likely driven by ignition pressure
405 and fire suppression (Balch et al. 2017). As human density increases from zero, ignition
406 pressure increases, but eventually landscapes become so urbanized, fragmented, and/or
407 fire-suppressed that wildfire risk decreases (Syphard et al. 2007; Bowman et al. 2011;
408 Bistinas et al. 2013; Knorr et al. 2013; Mcwethy et al. 2013; Syphard et al. 2017; Nagy et
409 al. 2018). At intermediate density, wildfire regimes respond to human ignition and altered
410 fuel distributions (Guyette, Muzika, and Dey 2002), but these responses depend on envi-
411 ronmental context and characteristics of the human population (Marlon et al. 2008; Li et
412 al. 2009). This model indicates that the combination of moderate to high human density
413 and dry conditions would nonlinearly increase the chance of an extreme fire event. Both
414 human density and dryness are expected to increase in the future across large swaths of
415 the U.S. (Lloyd, Sorichetta, and Tatem 2017; Stavros et al. 2014, Radeloff et al. (2010)),
416 with potential implications for human mortality, health risks from smoke and particulate
417 emission, and the financial burden of wildfire management (Reid et al. 2016; Radeloff et al.
418 2018).

419 This work points to promising directions for future predictive efforts. Default choices such
420 as Poisson and GPD distributions should be checked against alternative distributions.
421 Further, the predictive skill of this model seems to suggest that ordinary events provide
422 information on extremes, which would not be the case if the generative distribution of
423 extremes was completely unique. Previous case studies have identified that extremes or
424 anomalies in climatological drivers play a role in the evolution of extreme wildfires (Peter-
425 son et al. 2015), but for this work, monthly averages of climatological drivers over fairly
426 large spatial regions were used, which may smooth over anomalous or extreme conditions.
427 Enhancing the spatiotemporal resolution of predictive models could better represent cli-

428 matic and social drivers and provide localized insights to inform decision-making. This
429 raises computational challenges, but recent advances in distributed probabilistic computing
430 (Tran et al. 2017), efficient construction of spatiotemporal point processes (Shirota and
431 Banerjee 2018), and compact representations of nonlinear spatial interactions (Lee and
432 Durbán 2011) may provide solutions.

433 The Wallow Fire case study reveals at least one limitation of increasing the spatiotem-
434 poral resolution. When the model predictions are driven by covariates that are summa-
435 rized in space and time (e.g. a mean across an ecoregion in a month), summary values
436 may not represent conditions that are most relevant to an event. With a discrete space-
437 time segmentation, events can occur at the boundary of a spatiotemporal unit, e.g., if
438 a fire spreads into an adjacent ecoregion or ignites on the last day of the month. Large
439 wildfires can span months, and a model that only uses conditions upon ignition to pre-
440 dict total burned area can fail to account for conditions that change over the course of
441 the event. Modeling ignitions as a point process in continuous space and time (Brillinger,
442 Preisler, and Benoit 2003), and explicitly modeling subsequent fire duration and spread
443 could better separate conditions that ignite fires from those that affect propagation. Such
444 an approach might be amenable to including information on fuel continuity, which is likely
445 to limit the size of extremely large fires and did not factor into the current predictions
446 (Rollins, Morgan, and Swetnam 2002; Hargrove et al. 2000).

447 To the extent that a model reflects the generative process for extreme events, the decom-
448 position of contributions to the model's predictions may provide insight into attribution
449 for meteorological and anthropogenic drivers of extremes. However, a model trained to
450 represent a region-wide distribution of fire sizes will inevitably fail to capture local factors
451 that are relevant to specific events such as the Wallow Fire. If predicting the dynamics
452 of particular fire events is a goal, process-based models designed to model fire spread are
453 likely to be more appropriate than regional statistical models such as those developed
454 here.

455 This paper presents and evaluates a statistical approach to explain and predict extreme
456 wildfires that incorporates spatially varying non-linear effects. The model reveals consider-

457 able differences among ecoregions spanning the mountain west to the great plains, deserts,
458 and eastern forests, and suggests a non-negligible chance of extreme wildfires larger than
459 those seen in over the past 30 years in the contiguous U.S. Predictive approaches such as
460 this can inform decision-making by placing probabilistic bounds on the number of wildfires
461 and their sizes, while provide deeper insights into wildfire ecology.

462 **Acknowledgments**

463 We thank Mitzi Morris, Kyle Foreman, Daniel Simpson, Bob Carpenter, and Andrew Gel-
464 man for contributing to the implementation of an intrinsic autoregressive spatial prior
465 in Stan. We also thank two anonymous reviewers for their thoughtful comments, which
466 greatly improved the paper.

467 **Literature cited**

468 Abatzoglou, John T. 2013. “Development of Gridded Surface Meteorological Data for Eco-
469 logical Applications and Modelling.” *International Journal of Climatology* 33 (1). Wiley
470 Online Library: 121–31.

471 Abatzoglou, John T., and A. Park Williams. 2016. “Impact of Anthropogenic Climate
472 Change on Wildfire Across Western Us Forests.” *Proceedings of the National Academy of*
473 *Sciences* 113 (42). National Academy of Sciences: 11770–5. doi:10.1073/pnas.1607171113.

474 Allaire, JJ, Yihui Xie, Jonathan McPherson, Javier Luraschi, Kevin Ushey, Aron Atkins,
475 Hadley Wickham, Joe Cheng, and Winston Chang. 2018. *Rmarkdown: Dynamic Docu-*
476 *ments for R*. <https://CRAN.R-project.org/package=rmarkdown>.

477 Arnold, Jeffrey B. 2018. *Ggthemes: Extra Themes, Scales and Geoms for 'Ggplot2'*. <https://CRAN.R-project.org/package=ggthemes>.

479 Balch, Jennifer K, Bethany A Bradley, John T Abatzoglou, R Chelsea Nagy, Emily J

- 480 Fusco, and Adam L Mahood. 2017. “Human-Started Wildfires Expand the Fire Niche
481 Across the United States.” *Proceedings of the National Academy of Sciences* 114 (11). Na-
482 tional Acad Sciences: 2946–51.
- 483 Balshi, Michael S, A DAVID McGUIRE, Paul Duffy, Mike Flannigan, John Walsh, and
484 Jerry Melillo. 2009. “Assessing the Response of Area Burned to Changing Climate in
485 Western Boreal North America Using a Multivariate Adaptive Regression Splines (Mars)
486 Approach.” *Global Change Biology* 15 (3). Wiley Online Library: 578–600.
- 487 Banerjee, Sudipto, Bradley P Carlin, and Alan E Gelfand. 2014. *Hierarchical Modeling*
488 *and Analysis for Spatial Data*. CRC Press.
- 489 Barbero, R, JT Abatzoglou, EA Steel, and Narasimhan K Larkin. 2014. “Modeling Very
490 Large-Fire Occurrences over the Continental United States from Weather and Climate
491 Forcing.” *Environmental Research Letters* 9 (12). IOP Publishing: 124009.
- 492 Bates, Douglas, and Martin Maechler. 2018. *Matrix: Sparse and Dense Matrix Classes*
493 *and Methods*. <https://CRAN.R-project.org/package=Matrix>.
- 494 Beck, Christian, and EGD Cohen. 2003. “Superstatistics.” *Physica A: Statistical Mechan-*
495 *ics and Its Applications* 322. Elsevier: 267–75.
- 496 Bermudez, P de Zea, J Mendes, JMC Pereira, KF Turkman, and MJP Vasconcelos. 2009.
497 “Spatial and Temporal Extremes of Wildfire Sizes in Portugal (1984–2004).” *International*
498 *Journal of Wildland Fire* 18 (8). CSIRO Publishing: 983–91.
- 499 Besag, Julian, and Charles Kooperberg. 1995. “On Conditional and Intrinsic Autoregres-
500 sions.” *Biometrika* 82 (4). Oxford University Press: 733–46.
- 501 Bistinas, Ioannis, Duarte Oom, Ana C. L. Sá, Sandy P. Harrison, I. Colin Prentice, and
502 José M. C. Pereira. 2013. “Relationships between Human Population Density and Burned
503 Area at Continental and Global Scales.” *PLoS ONE*. doi:10.1371/journal.pone.0081188.
- 504 Bivand, Roger, and Gianfranco Piras. 2015. “Comparing Implementations of Estimation
505 Methods for Spatial Econometrics.” In. American Statistical Association.
- 506 Bivand, Roger, Tim Keitt, and Barry Rowlingson. 2018. *Rgdal: Bindings for the 'Geospa-*

- 507 *tial' Data Abstraction Library*. <https://CRAN.R-project.org/package=rgdal>.
- 508 Boettiger, Carl. 2015. "An Introduction to Docker for Reproducible Research." *ACM*
509 *SIGOPS Operating Systems Review* 49 (1). ACM: 71–79.
- 510 Bowman, David MJS, Jennifer Balch, Paulo Artaxo, William J Bond, Mark A Cochrane,
511 Carla M D'antonio, Ruth DeFries, et al. 2011. "The Human Dimension of Fire Regimes on
512 Earth." *Journal of Biogeography* 38 (12). Wiley Online Library: 2223–36.
- 513 Brezger, Andreas, and Stefan Lang. 2006. "Generalized Structured Additive Regression
514 Based on Bayesian P-Splines." *Computational Statistics & Data Analysis* 50 (4). Elsevier:
515 967–91.
- 516 Brezger, Andreas, and Winfried J Steiner. 2008. "Monotonic Regression Based on
517 Bayesian P-Splines: An Application to Estimating Price Response Functions from
518 Store-Level Scanner Data." *Journal of Business & Economic Statistics* 26 (1). Taylor &
519 Francis: 90–104.
- 520 Brillinger, David R, Haiganoush K Preisler, and John W Benoit. 2003. "Risk Assessment:
521 A Forest Fire Example." *Lecture Notes-Monograph Series*. JSTOR, 177–96.
- 522 Brooks, Stephen P, and Andrew Gelman. 1998. "General Methods for Monitoring Conver-
523 gence of Iterative Simulations." *Journal of Computational and Graphical Statistics* 7 (4).
524 Taylor & Francis: 434–55.
- 525 Carpenter, Bob, Andrew Gelman, Matt Hoffman, Daniel Lee, Ben Goodrich, Michael
526 Betancourt, Michael A Brubaker, Jiqiang Guo, Peter Li, and Allen Riddell. 2016. "Stan:
527 A Probabilistic Programming Language." *Journal of Statistical Software* 20: 1–37.
- 528 Coles, S. 2014. *An Introduction to Statistical Modeling of Extreme Values*. Springer. <https://books.google.com/books?id=G-D-sgEACAAJ>.
- 530 Coles, Stuart, Joanna Bawa, Lesley Trenner, and Pat Dorazio. 2001. *An Introduction to*
531 *Statistical Modeling of Extreme Values*. Vol. 208. Springer.
- 532 Coles, Stuart, Luis Raúl Pericchi, and Scott Sisson. 2003. "A Fully Probabilistic Approach

- 533 to Extreme Rainfall Modeling.” *Journal of Hydrology* 273 (1-4). Elsevier: 35–50.
- 534 Cox, David Roxbee, and Valerie Isham. 1980. *Point Processes*. Vol. 12. CRC Press.
- 535 Daly, Christopher, Michael Halbleib, Joseph I Smith, Wayne P Gibson, Matthew K
536 Doggett, George H Taylor, Jan Curtis, and Phillip P Pasteris. 2008. “Physiographically
537 Sensitive Mapping of Climatological Temperature and Precipitation Across the Contermi-
538 nous United States.” *International Journal of Climatology* 28 (15). Wiley Online Library:
539 2031–64.
- 540 Davison, Anthony C, and Richard L Smith. 1990. “Models for Exceedances over High
541 Thresholds.” *Journal of the Royal Statistical Society. Series B (Methodological)*. JSTOR,
542 393–442.
- 543 Dennison, Philip E, Simon C Brewer, James D Arnold, and Max A Moritz. 2014. “Large
544 Wildfire Trends in the Western United States, 1984–2011.” *Geophysical Research Letters* 41
545 (8). Wiley Online Library: 2928–33.
- 546 Diaz, John M. 2012. “Economic Impacts of Wildfire.” *Southern Fire Exchange*.
- 547 Díaz-Avalos, Carlos, Pablo Juan, and Laura Serra-Saurina. 2016. “Modeling Fire Size of
548 Wildfires in Castellon (Spain), Using Spatiotemporal Marked Point Processes.” *Forest
549 Ecology and Management* 381. Elsevier: 360–69.
- 550 Dubey, Satya D. 1970. “Compound Gamma, Beta and F Distributions.” *Metrika* 16 (1).
551 Springer: 27–31.
- 552 Eidenshink, J, B Schwind, K Brewer, ZL Zhu, B Quayle, and S Howard. 2007. “A Project
553 for Monitoring Trends in Burn Severity.” *Nutrition and Cancer* 58 (1): 28–34.
- 554 Flannigan, Mike D., Meg A. Krawchuk, William J. de Groot, B. Mike Wotton, and
555 Lynn M. Gowman. 2009. “Implications of Changing Climate for Global Wildland
556 Fire.” Journal Article. *International Journal of Wildland Fire* 18 (5): 483–507.
557 doi:<http://dx.doi.org/10.1071/WF08187>.
- 558 Fosberg, Michael A. 1978. “Weather in Wildland Fire Management: The Fire Weather

- 559 Index.” *US for Serv Reprints of Articles by FS Employees*.
- 560 Gelman, A., J.B. Carlin, H.S. Stern, D.B. Dunson, A. Vehtari, and D.B. Rubin. 2013.
561 *Bayesian Data Analysis, Third Edition*. Chapman & Hall/Crc Texts in Statistical Science.
562 Taylor & Francis. <https://books.google.com/books?id=ZXL6AQAAQBAJ>.
- 563 Gelman, Andrew, Xiao-Li Meng, and Hal Stern. 1996. “Posterior Predictive Assessment of
564 Model Fitness via Realized Discrepancies.” *Statistica Sinica*. JSTOR, 733–60.
- 565 Goodrick, Scott L. 2002. “Modification of the Fosberg Fire Weather Index to Include
566 Drought.” *International Journal of Wildland Fire* 11 (4). CSIRO: 205–11.
- 567 Golemund, Garrett, and Hadley Wickham. 2011. “Dates and Times Made Easy with
568 lubridate.” *Journal of Statistical Software* 40 (3): 1–25. [http://www.jstatsoft.org/v40/
569 i03/](http://www.jstatsoft.org/v40/i03/).
- 570 Guyette, R. P., R. M Muzika, and D. C. Dey. 2002. “Dynamics of an Anthropogenic Fire
571 Regime.” *Ecosystems* 5: 472–86. doi:10.1007/s10021-002-0115-7.
- 572 Hargrove, William W, RH Gardner, MG Turner, WH Romme, and DG Despain. 2000.
573 “Simulating Fire Patterns in Heterogeneous Landscapes.” *Ecological Modelling* 135 (2-3).
574 Elsevier: 243–63.
- 575 Hernandez, Charles, C Keribin, P Drobinski, and S Turquety. 2015. “Statistical Modelling
576 of Wildfire Size and Intensity: A Step Toward Meteorological Forecasting of Summer Ex-
577 treme Fire Risk.” In *Annales Geophysicae*, 33:1495–1506. 12.
- 578 Hijmans, Robert J. 2017. *Raster: Geographic Data Analysis and Modeling*. [https://CRAN.
579 R-project.org/package=raster](https://CRAN.R-project.org/package=raster).
- 580 Hoffman, Matthew D, and Andrew Gelman. 2014. “The No-U-Turn Sampler: Adaptively
581 Setting Path Lengths in Hamiltonian Monte Carlo.” *Journal of Machine Learning Re-
582 search* 15 (1): 1593–1623.
- 583 Hosking, Jonathan RM, and James R Wallis. 1987. “Parameter and Quantile Estimation

- 584 for the Generalized Pareto Distribution.” *Technometrics* 29 (3). Taylor & Francis: 339–49.
- 585 Jiang, Yueyang, and Qianlai Zhuang. 2011. “Extreme Value Analysis of Wildfires in Cana-
586 dian Boreal Forest Ecosystems.” *Canadian Journal of Forest Research* 41 (9). NRC Re-
587 search Press: 1836–51.
- 588 Joseph, Max. 2018. “MbJoseph/Wildfire-Extremes: First Release.” doi:10.5281/zenodo.1326858.
- 589 Kneib, Thomas, Torsten Hothorn, and Gerhard Tutz. 2009. “Variable Selection and Model
590 Choice in Geoadditive Regression Models.” *Biometrics* 65 (2). Wiley Online Library: 626–
591 34.
- 592 Knorr, W, T Kaminski, A Arneth, and U Weber. 2013. “Impact of human population
593 density on fire frequency at the global scale Impact of human population density on fire
594 frequency at the global scale Impact of human population density on fire frequency at the
595 global scale.” *Biogeosciences Discuss* 10: 15735–78. doi:10.5194/bgd-10-15735-2013.
- 596 Kochi, Ikuho, Geoffrey H Donovan, Patricia A Champ, and John B Loomis. 2010. “The
597 Economic Cost of Adverse Health Effects from Wildfire-Smoke Exposure: A Review.” *In-
598 ternational Journal of Wildland Fire* 19 (7). CSIRO: 803–17.
- 599 Krawchuk, Meg A, Max A Moritz, Marc-André Parisien, Jeff Van Dorn, and Katharine
600 Hayhoe. 2009. “Global Pyrogeography: The Current and Future Distribution of Wildfire.”
601 *PloS One* 4 (4). Public Library of Science: e5102.
- 602 Krawchuk, Meg A., and Max A. Moritz. 2011. “Constraints on global fire activity vary
603 across a resource gradient.” *Ecology* 92 (1): 121–32. doi:10.1890/09-1843.1.
- 604 Kucukelbir, Alp, Rajesh Ranganath, Andrew Gelman, and David Blei. 2015. “Automatic
605 Variational Inference in Stan.” In *Advances in Neural Information Processing Systems*,
606 568–76.
- 607 Lambert, Diane. 1992. “Zero-Inflated Poisson Regression, with an Application to Defects
608 in Manufacturing.” *Technometrics* 34 (1). Taylor & Francis: 1–14.
- 609 Lee, Dae-Jin, and María Durbán. 2011. “P-Spline Anova-Type Interaction Models for
610 Spatio-Temporal Smoothing.” *Statistical Modelling* 11 (1). SAGE Publications Sage India:

- 611 New Delhi, India: 49–69.
- 612 Li, Li-Ming, Wei-Guo Song, Jian Ma, and Kohyu Satoh. 2009. “Artificial neural network
613 approach for modeling the impact of population density and weather parameters on for-
614 est fire risk.” *International Journal of Wildland Fire* 18 (6). CSIRO PUBLISHING: 640.
615 doi:10.1071/WF07136.
- 616 Lloyd, Christopher T, Alessandro Sorichetta, and Andrew J Tatem. 2017. “High Reso-
617 lution Global Gridded Data for Use in Population Studies.” *Scientific Data* 4. Nature
618 Publishing Group: 170001.
- 619 Marani, Marco, and Massimiliano Ignaccolo. 2015. “A Metastatistical Approach to Rain-
620 fall Extremes.” *Advances in Water Resources* 79. Elsevier: 121–26.
- 621 Marlon, J. R., P. J. Bartlein, C. Carcaillet, D. G. Gavin, S. P. Harrison, P. E. Higuera,
622 F. Joos, M. J. Power, and I. C. Prentice. 2008. “Climate and human influences on global
623 biomass burning over the past two millennia.” *Nature Geoscience*. doi:10.1038/ngeo313.
- 624 McLaughlin, Steven P, and Janice E Bowers. 1982. “Effects of Wildfire on a Sonoran
625 Desert Plant Community.” *Ecology*. JSTOR, 246–48.
- 626 Mcwethy, D. B., P. E. Higuera, C. Whitlock, T. T. Veblen, D. M J S Bowman, G. J. Cary,
627 S. G. Haberle, et al. 2013. “A conceptual framework for predicting temperate ecosystem
628 sensitivity to human impacts on fire regimes.” *Global Ecology and Biogeography* 22 (8):
629 900–912.
- 630 Mendes, Jorge M, Patrícia Cortés de Zea Bermudez, José Pereira, KF Turkman, and MJP
631 Vasconcelos. 2010. “Spatial Extremes of Wildfire Sizes: Bayesian Hierarchical Models for
632 Extremes.” *Environmental and Ecological Statistics* 17 (1). Springer: 1–28.
- 633 Moritz, Max A, Marc-André Parisien, Enric Batllori, Meg A Krawchuk, Jeff Van Dorn,
634 David J Ganz, and Katharine Hayhoe. 2012. “Climate Change and Disruptions to Global
635 Fire Activity.” *Ecosphere* 3 (6). Wiley Online Library: 1–22.
- 636 Nagy, R, Emily Fusco, Bethany Bradley, John T Abatzoglou, and Jennifer Balch. 2018.
637 “Human-Related Ignitions Increase the Number of Large Wildfires Across Us Ecoregions.”

- 638 *Fire* 1 (1). Multidisciplinary Digital Publishing Institute: 4.
- 639 Nauslar, Nicholas, John Abatzoglou, and Patrick Marsh. 2018. “The 2017 North Bay and
640 Southern California Fires: A Case Study.” *Fire* 1 (1). Multidisciplinary Digital Publishing
641 Institute: 18.
- 642 Neuwirth, Erich. 2014. *RColorBrewer: ColorBrewer Palettes*. [https://CRAN.R-project.
643 org/package=RColorBrewer](https://CRAN.R-project.org/package=RColorBrewer).
- 644 Omernik, James M. 1987. “Ecoregions of the Conterminous United States.” *Annals of the
645 Association of American Geographers* 77 (1). Taylor & Francis: 118–25.
- 646 Omernik, James M, and Glenn E Griffith. 2014. “Ecoregions of the Conterminous United
647 States: Evolution of a Hierarchical Spatial Framework.” *Environmental Management* 54
648 (6). Springer: 1249–66.
- 649 Pebesma, Edzer. 2018. *Sf: Simple Features for R*. [https://CRAN.R-project.org/package=
650 sf](https://CRAN.R-project.org/package=sf).
- 651 Pechony, O, and DT Shindell. 2009. “Fire Parameterization on a Global Scale.” *Journal of
652 Geophysical Research: Atmospheres* 114 (D16). Wiley Online Library.
- 653 Pechony, Olga, and Drew T Shindell. 2010. “Driving Forces of Global Wildfires over the
654 Past Millennium and the Forthcoming Century.” *Proceedings of the National Academy of
655 Sciences* 107 (45). National Acad Sciences: 19167–70.
- 656 Pedersen, Thomas Lin. 2017. *Patchwork: The Composer of Ggplots*. [https://github.com/
657 thomasp85/patchwork](https://github.com/thomasp85/patchwork).
- 658 Peltola, Tomi, Aki S Havulinna, Veikko Salomaa, and Aki Vehtari. 2014. “Hierarchical
659 Bayesian Survival Analysis and Projective Covariate Selection in Cardiovascular Event
660 Risk Prediction.” In *Proceedings of the Eleventh Uai Conference on Bayesian Modeling
661 Applications Workshop-Volume 1218*, 79–88. CEUR-WS. org.
- 662 Pernin, Peter. 1971. “The Great Peshtigo Fire: An Eyewitness Account.” *The Wisconsin*

663 *Magazine of History*. JSTOR, 246–72.

664 Peterson, David A, Edward J Hyer, James R Campbell, Michael D Fromm, Johnathan W
665 Hair, Carolyn F Butler, and Marta A Fenn. 2015. “The 2013 Rim Fire: Implications for
666 Predicting Extreme Fire Spread, Pyroconvection, and Smoke Emissions.” *Bulletin of the*
667 *American Meteorological Society* 96 (2): 229–47.

668 Piironen, Juho, Aki Vehtari, and others. 2017. “Sparsity Information and Regularization
669 in the Horseshoe and Other Shrinkage Priors.” *Electronic Journal of Statistics* 11 (2). The
670 Institute of Mathematical Statistics; the Bernoulli Society: 5018–51.

671 Preisler, Haiganoush K, and Anthony L Westerling. 2007. “Statistical Model for Fore-
672 casting Monthly Large Wildfire Events in Western United States.” *Journal of Applied*
673 *Meteorology and Climatology* 46 (7): 1020–30.

674 Preisler, Haiganoush K, David R Brillinger, Robert E Burgan, and JW Benoit. 2004.
675 “Probability Based Models for Estimation of Wildfire Risk.” *International Journal of Wild-*
676 *land Fire* 13 (2). CSIRO: 133–42.

677 Quionero-Candela, Joaquin, Masashi Sugiyama, Anton Schwaighofer, and Neil D Lawrence.
678 2009. *Dataset Shift in Machine Learning*. The MIT Press.

679 R Core Team. 2017. *R: A Language and Environment for Statistical Computing*. Vienna,
680 Austria: R Foundation for Statistical Computing. <https://www.R-project.org/>.

681 ———. 2018. *R: A Language and Environment for Statistical Computing*. Vienna, Austria:
682 R Foundation for Statistical Computing. <https://www.R-project.org/>.

683 Radeloff, Volker C, David P Helmers, H Anu Kramer, Miranda H Mockrin, Patricia M
684 Alexandre, Avi Bar-Massada, Van Butsic, et al. 2018. “Rapid Growth of the Us Wildland-
685 Urban Interface Raises Wildfire Risk.” *Proceedings of the National Academy of Sciences*
686 115 (13). National Acad Sciences: 3314–9.

687 Radeloff, Volker C, Susan I Stewart, Todd J Hawbaker, Urs Gimmi, Anna M Pidgeon,
688 Curtis H Flather, Roger B Hammer, and David P Helmers. 2010. “Housing Growth in and
689 Near United States Protected Areas Limits Their Conservation Value.” *Proceedings of the*

- 690 *National Academy of Sciences* 107 (2). National Acad Sciences: 940–45.
- 691 Ramsay, James O, and others. 1988. “Monotone Regression Splines in Action.” *Statistical*
692 *Science* 3 (4). Institute of Mathematical Statistics: 425–41.
- 693 Reed, William J, and Kevin S McKelvey. 2002. “Power-Law Behaviour and Parametric
694 Models for the Size-Distribution of Forest Fires.” *Ecological Modelling* 150 (3). Elsevier:
695 239–54.
- 696 Reid, Colleen E, Michael Brauer, Fay H Johnston, Michael Jerrett, John R Balmes, and
697 Catherine T Elliott. 2016. “Critical Review of Health Impacts of Wildfire Smoke Expo-
698 sure.” *Environmental Health Perspectives* 124 (9). National Institute of Environmental
699 Health Science: 1334.
- 700 Rogers, Brendan M., Ronald P. Neilson, Ray Drapek, James M. Lenihan, John R. Wells,
701 Dominique Bachelet, and Beverly E. Law. 2011. “Impacts of Climate Change on Fire
702 Regimes and Carbon Stocks of the U.S. Pacific Northwest.” *Journal of Geophysical Re-*
703 *search: Biogeosciences* 116 (G3): n/a–n/a. doi:10.1029/2011JG001695.
- 704 Rollins, Matthew G, Penelope Morgan, and Thomas Swetnam. 2002. “Landscape-Scale
705 Controls over 20th Century Fire Occurrence in Two Large Rocky Mountain (Usa) Wilder-
706 ness Areas.” *Landscape Ecology* 17 (6). Springer: 539–57.
- 707 Schoenberg, Frederic Paik, Roger Peng, and James Woods. 2003. “On the Distribution of
708 Wildfire Sizes.” *Environmetrics* 14 (6). Wiley Online Library: 583–92.
- 709 Serra, Laura, Marc Saez, Pablo Juan, Diego Varga, and Jorge Mateu. 2014. “A Spatio-
710 Temporal Poisson Hurdle Point Process to Model Wildfires.” *Stochastic Environmental*
711 *Research and Risk Assessment* 28 (7). Springer: 1671–84.
- 712 Serra, Laura, Marc Saez, Jorge Mateu, Diego Varga, Pablo Juan, Carlos Díaz-Ávalos, and
713 Håvard Rue. 2014. “Spatio-Temporal Log-Gaussian Cox Processes for Modelling Wildfire
714 Occurrence: The Case of Catalonia, 1994–2008.” *Environmental and Ecological Statistics*
715 21 (3). Springer: 531–63.
- 716 Shirota, Shinichiro, and Sudipto Banerjee. 2018. “Scalable Inference for Space-Time Gaus-

- 717 sian Cox Processes.” *arXiv Preprint arXiv:1802.06151*.
- 718 Slowikowski, Kamil. 2018. *Ggrepel: Automatically Position Non-Overlapping Text Labels*
719 *with 'Ggplot2'*. <https://CRAN.R-project.org/package=ggrepel>.
- 720 Solymos, Peter, and Zygmunt Zawadzki. 2018. *Pbapply: Adding Progress Bar to '*Apply'*
721 *Functions*. <https://CRAN.R-project.org/package=pbapply>.
- 722 Stallman, Richard M., Roland McGrath, and Paul D. Smith. 2004. *GNU Make: A Pro-*
723 *gram for Directing Recompilation, for Version 3.81*. Free Software Foundation.
- 724 Stan Development Team. 2018. “RStan: The R Interface to Stan.” <http://mc-stan.org/>.
- 725 Stavros, E Natasha, John T Abatzoglou, Donald McKenzie, and Narasimhan K Larkin.
726 2014. “Regional Projections of the Likelihood of Very Large Wildland Fires Under a
727 Changing Climate in the Contiguous Western United States.” *Climatic Change* 126 (3-
728 4). Springer: 455–68.
- 729 Syphard, Alexandra D. AD, Volker C. VC Radeloff, Jon E. Keeley, Todd J. Hawbaker,
730 Murray K. Clayton, Susan I. Stewart, and Roger B. Hammer. 2007. “Human influence on
731 California fire regimes.” *Ecological Applications* 17 (5): 1388–1402.
- 732 Syphard, Alexandra D., Jon E. Keeley, Anne H. Pfaff, and Ken Ferschweiler.
733 2017. “Human presence diminishes the importance of climate in driving fire ac-
734 tivity across the United States.” *Proceedings of the National Academy of Sciences*.
735 doi:10.1073/pnas.1713885114.
- 736 Tedim, Fantina, Vittorio Leone, Malik Amraoui, Christophe Bouillon, Michael R Coughlan,
737 Giuseppe M Delogu, Paulo M Fernandes, et al. 2018. “Defining Extreme Wildfire Events:
738 Difficulties, Challenges, and Impacts.” *Fire* 1 (1). Multidisciplinary Digital Publishing
739 Institute: 9.
- 740 Tran, Dustin, Matthew D Hoffman, Rif A Saurous, Eugene Brevdo, Kevin Murphy, and
741 David M Blei. 2017. “Deep Probabilistic Programming.” *arXiv Preprint arXiv:1701.03757*.
- 742 Vilar, Lara, Douglas G Woolford, David L Martell, and M Pilar Martín. 2010. “A Model
743 for Predicting Human-Caused Wildfire Occurrence in the Region of Madrid, Spain.” *Inter-*

- 744 *national Journal of Wildland Fire* 19 (3). CSIRO: 325–37.
- 745 Westerling, AL, BP Bryant, HK Preisler, TP Holmes, HG Hidalgo, T Das, and SR
746 Shrestha. 2011. “Climate Change and Growth Scenarios for California Wildfire.” *Climatic*
747 *Change* 109 (1). Springer: 445–63.
- 748 Westerling, Anthony LeRoy. 2016. “Increasing Western Us Forest Wildfire Activity: Sensi-
749 tivity to Changes in the Timing of Spring.” *Phil. Trans. R. Soc. B* 371 (1696). The Royal
750 Society: 20150178.
- 751 Wickham, Hadley. 2017a. *Assertthat: Easy Pre and Post Assertions*. [https://CRAN.](https://CRAN.R-project.org/package=assertthat)
752 [R-project.org/package=assertthat](https://CRAN.R-project.org/package=assertthat).
- 753 ———. 2017b. *Tidyverse: Easily Install and Load the 'Tidyverse'*. [https://CRAN.](https://CRAN.R-project.org/package=tidyverse)
754 [R-project.org/package=tidyverse](https://CRAN.R-project.org/package=tidyverse).
- 755 Wiitala, Marc R. 1999. “Assessing the Risk of Cumulative Burned Acreage Using the Pois-
756 son Probability Model.” *Fire Economics, Planning, and Policy: Bottom Lines*. Citeseer,
757 51.
- 758 Wilke, Claus O. 2017. *Cowplot: Streamlined Plot Theme and Plot Annotations for 'Gg-*
759 *plot2'*. <https://CRAN.R-project.org/package=cowplot>.
- 760 Williams, Jerry. 2013. “Exploring the Onset of High-Impact Mega-Fires Through a Forest
761 Land Management Prism.” *Forest Ecology and Management* 294. Elsevier: 4–10.
- 762 Wood, S.N. 2017. *Generalized Additive Models: An Introduction with R*. 2nd ed. Chapman;
763 Hall/CRC.
- 764 Woolford, DG, DR Bellhouse, WJ Braun, Ch B Dean, DL Martell, and J Sun. 2011. “A
765 Spatio-Temporal Model for People-Caused Forest Fire Occurrence in the Romeo Malette
766 Forest.” *Journal of Environmental Statistics* 2: 2–16.
- 767 Woolford, Douglas G, CB Dean, David L Martell, Jiguo Cao, and BM Wotton. 2014.
768 “Lightning-Caused Forest Fire Risk in Northwestern Ontario, Canada, Is Increasing and
769 Associated with Anomalies in Fire Weather.” *Environmetrics* 25 (6). Wiley Online Library:

770 406–16.

771 Yao, Yuling, Aki Vehtari, Daniel Simpson, Andrew Gelman, and others. 2017. “Using
772 Stacking to Average Bayesian Predictive Distributions.” *Bayesian Analysis*. International
773 Society for Bayesian Analysis.

774 Zeileis, Achim, and Gabor Grothendieck. 2005. “Zoo: S3 Infrastructure for Reg-
775 ular and Irregular Time Series.” *Journal of Statistical Software* 14 (6): 1–27.
776 doi:10.18637/jss.v014.i06.

777 Zorzetto, E, G Botter, and M Marani. 2016. “On the Emergence of Rainfall Extremes
778 from Ordinary Events.” *Geophysical Research Letters* 43 (15). Wiley Online Library: 8076–
779 82.

780 Tables

Table 1. Performance of count models on the test set in descending order. Posterior means are provided with standard deviations in parentheses.

Model	Holdout log likelihood
ZI Negative binomial	-3671 (70)
ZI Poisson	-4093 (77)
Negative binomial	-4298 (114)
Poisson	-4572 (139)

Table 2. Performance of burned area models on the test set in descending order. Posterior means are provided with standard deviations in parentheses.

Model	Holdout log likelihood
Lognormal	-26341 (43)
Generalized Pareto	-26377 (45)
Tapered Pareto	-26386 (49)
Weibull	-27592 (236)
Gamma	-30675 (993)

781 **Figures**

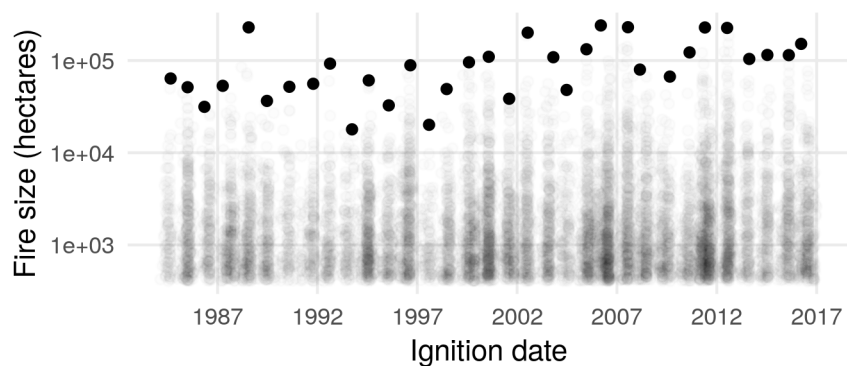


Figure 1. Sizes of wildfires over 405 hectares in the contiguous United States, from the Monitoring Trends in Burn Severity multiagency program. Each point represents a fire event, and the largest fires for each year (the block maxima) are shown as solid black points.

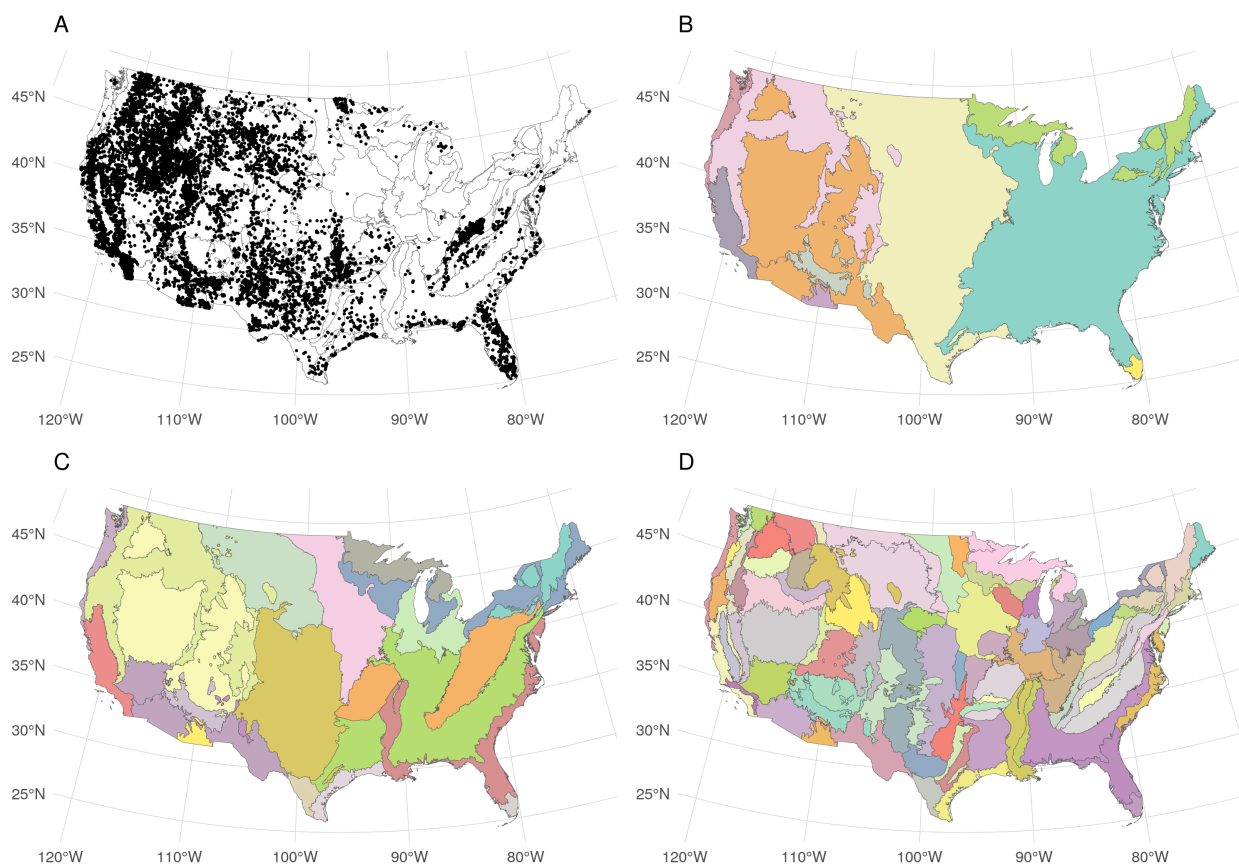


Figure 2. A. Large wildfire ignition locations are shown as points across the study region. Colors in panels B, C, and D show level 1, 2, and 3 ecoregions respectively.

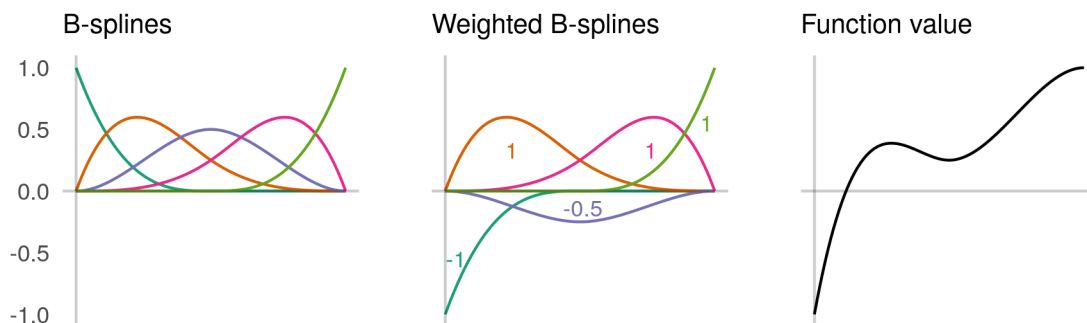


Figure 3. Conceptual figure to illustrate the use of B-splines to construct nonlinear functions. In the left panel, five B-spline vectors are shown, which map values of an input variable (on the x-axis) to a value on the y-axis. The middle panel shows the same B-spline vectors, but weighted (multiplied) by real numbers, with the weights illustrated as annotations. These weighted B-spline vectors are summed to produce the values of a nonlinear function (right panel).

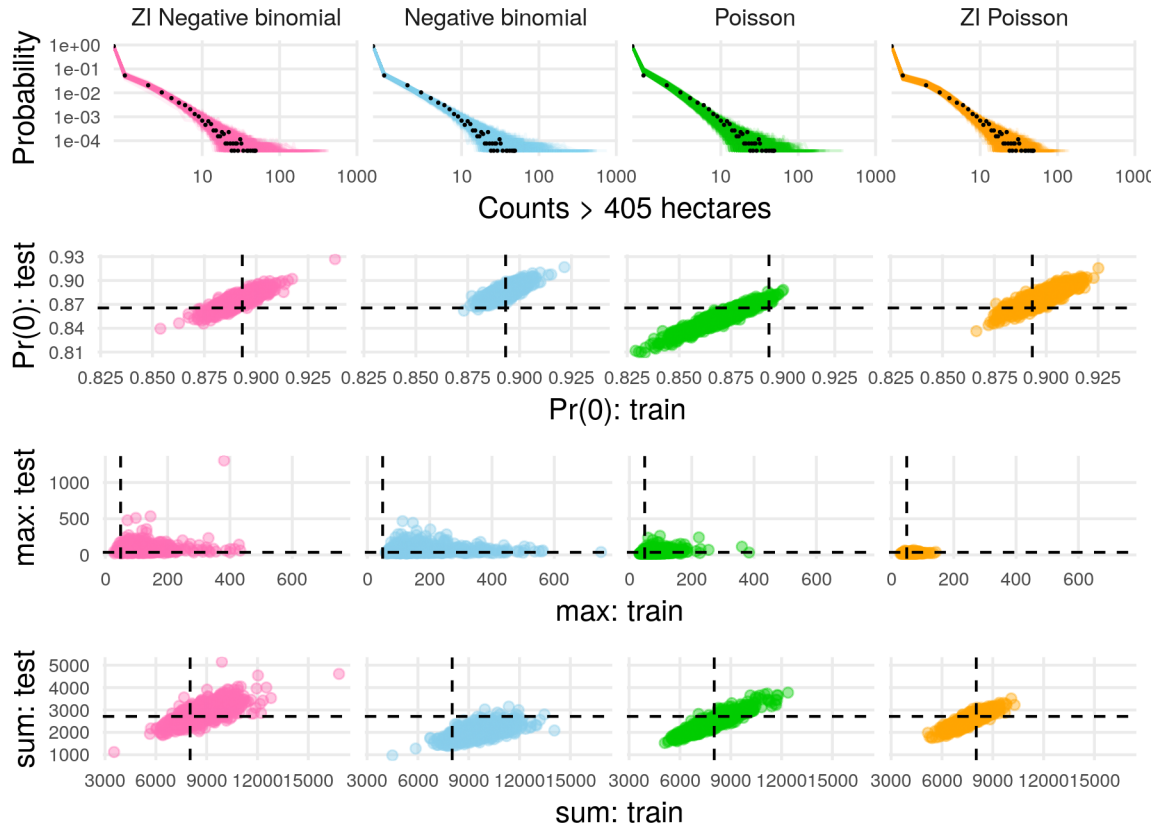


Figure 4. Count predictive checks. Row one shows observed count frequencies as black points and predicted frequencies as lines. Rows two, three, and four show predicted proportions of zeros, maxima, and sums (respectively) in the training and test data, with empirical values as dashed lines. Rows two through four facilitate comparison of performance on training and test sets. Ideally, model predictions cluster around the dashed lines for both the training (x-axis direction) and test (y-axis direction) sets, leading to a tight cluster of points at the intersection of the dashed lines.

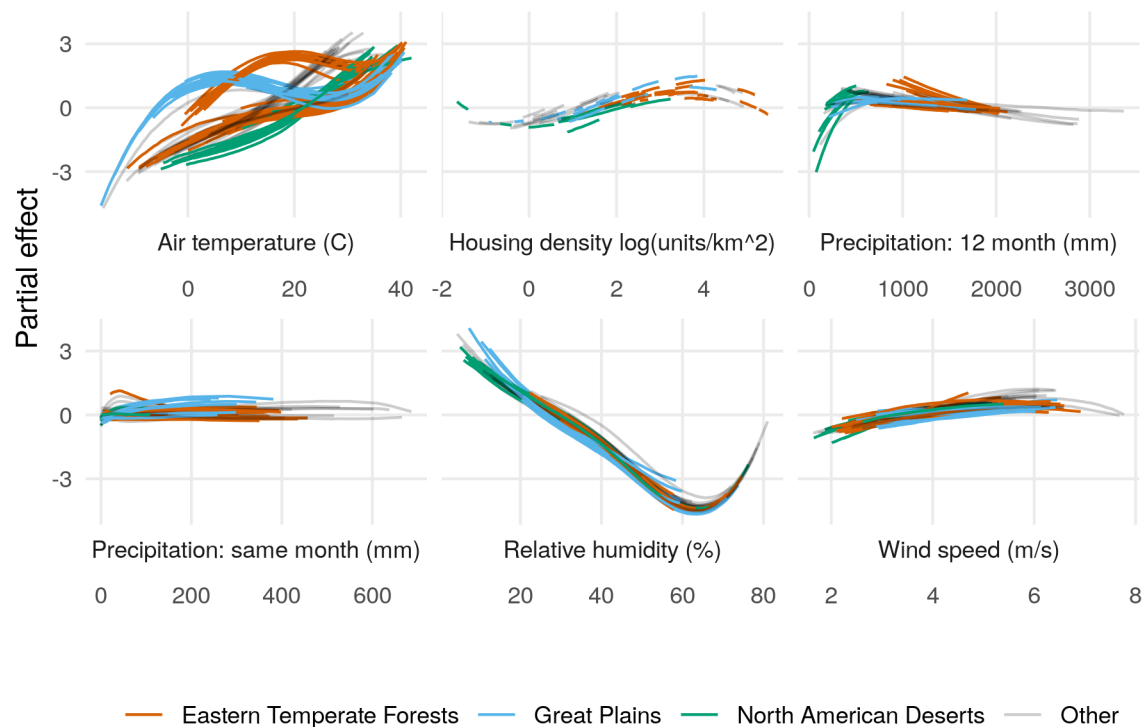


Figure 5. Partial effects on the log-transformed negative binomial mean component of the zero-inflated negative binomial model for each level 3 ecoregion, colored by level 1 ecoregion. Lines are posterior medians. Results are similar for the zero-inflation component.

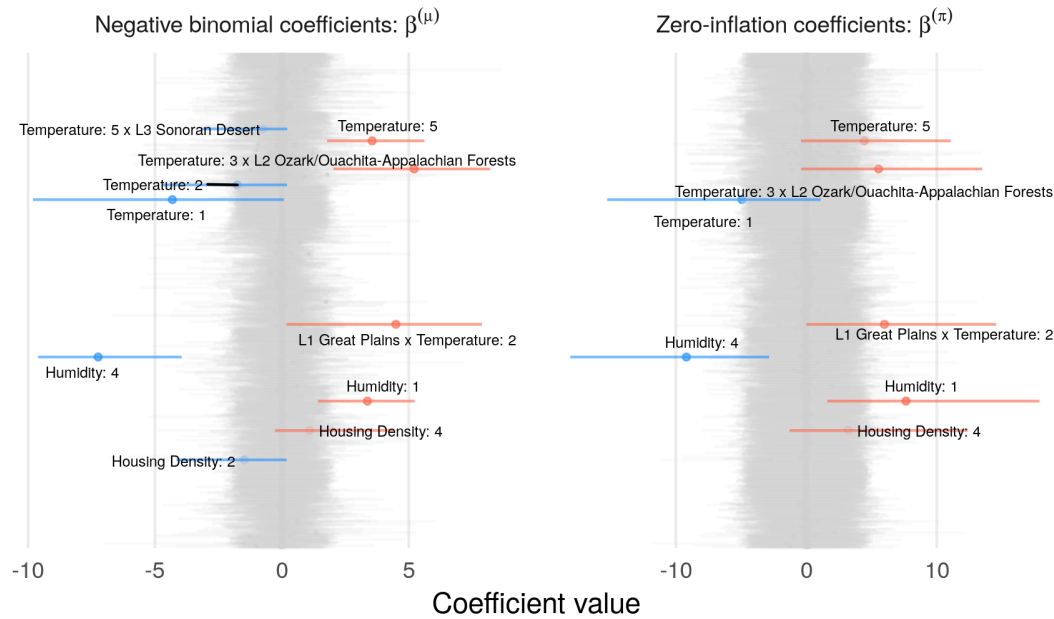


Figure 6. Caterpillar plots of zero inflated negative binomial model coefficients, $\beta^{(\mu)}$ (left) and $\beta^{(\pi)}$ (right). Horizontal line segments denote 95% credible intervals. Grey segments indicate coefficients with a less than 87% posterior probability of being positive or negative, and colored segments indicate coefficients that are probably positive (red) or negative (blue). B-spline vectors are indicated by colons, e.g., Humidity:1 indicates the first basis vector corresponding to humidity. Interactions between variables a and b are represented as a x b. Level 1 ecoregions are represented by L1 ecoregion name, and L2 and L3 indicate level 2 and 3 ecoregions.

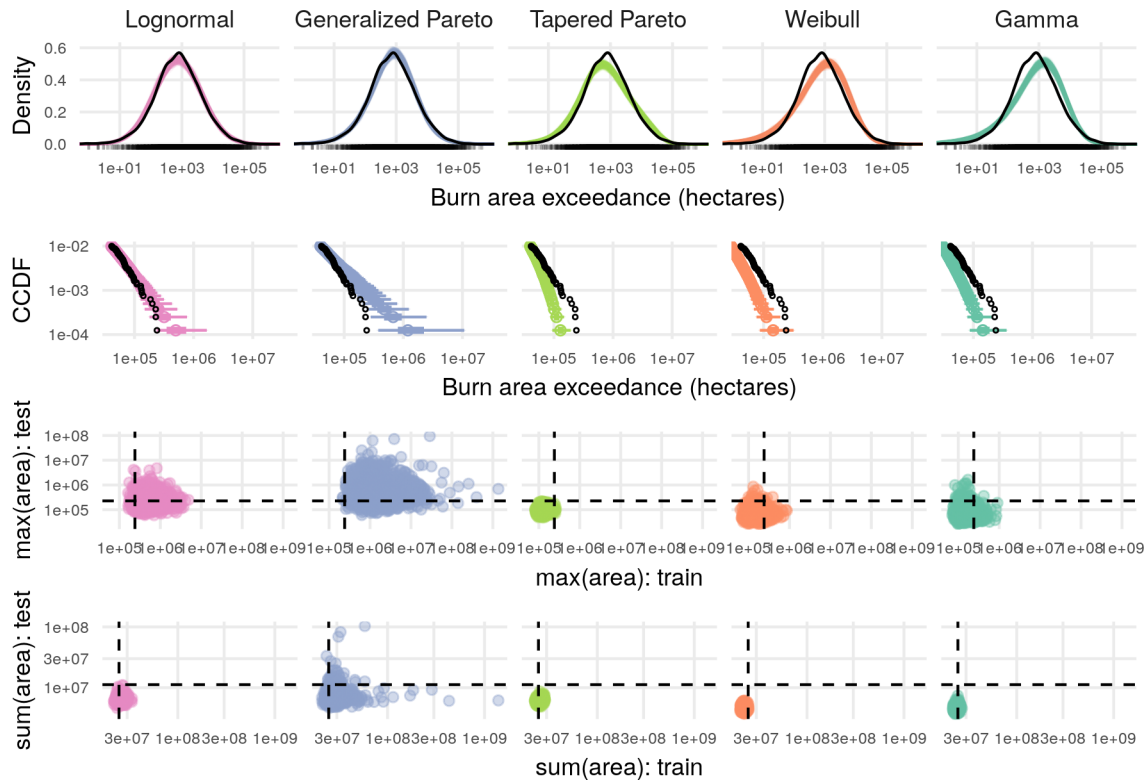


Figure 7. Predictive checks for burned area models. The top row shows predicted density in color and empirical density for the training set in black, which reveals overall lack of fit for the gamma and Weibull models. Row two shows the complementary cumulative distribution function (CCDF) at the tails, with 95% and 50% prediction intervals shown in color and observed data as black points, which shows that the Generalized Pareto distribution predicts values that are too extreme. The third and fourth rows show checks for maximum and total burned areas in the training and test set, with observed values as dashed lines and posterior draws as colored points. These final two rows facilitate checks for summary statistics on both the training and test set, with the ideal model generating predictions (colored points) clustered close to where the dashed lines intersect.

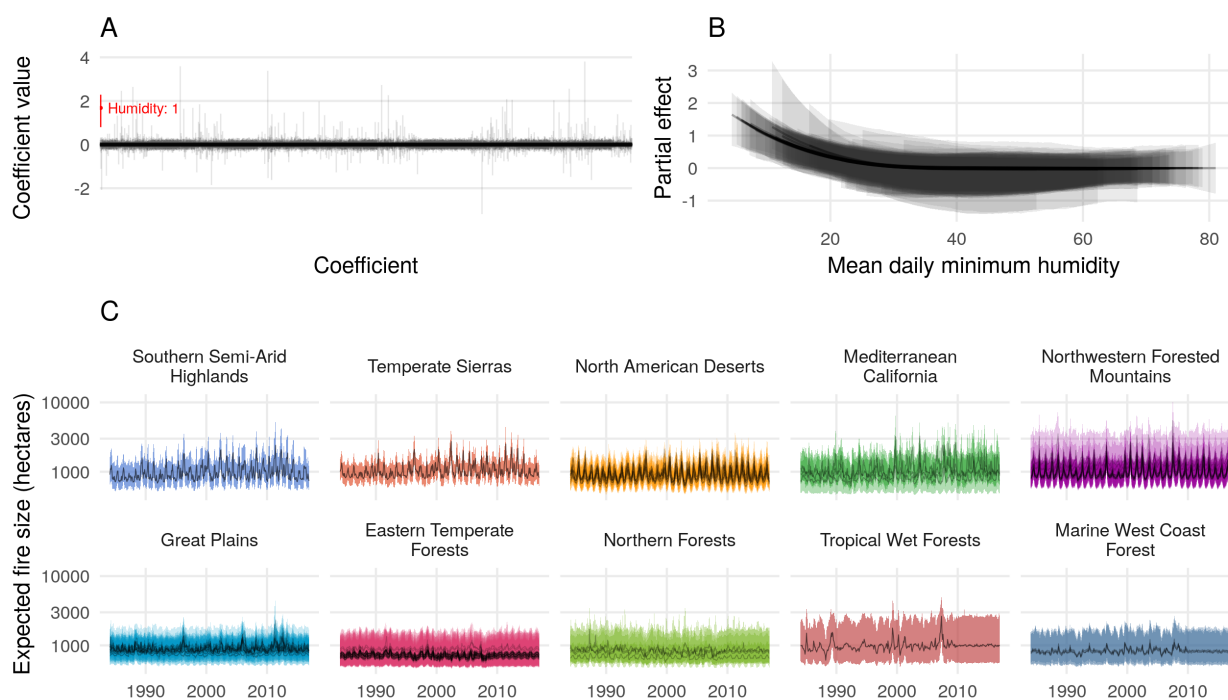


Figure 8. **A.** Estimated posterior medians and 95% credible intervals for each of the 3,473 coefficients associated with expected burned area. Only one coefficient - the first basis vector for humidity - had a 95% credible interval that excluded zero, shown in red. This effect is visualized in **B.** Partial effects of mean daily minimum humidity for each level 3 ecoregion, with posterior medians drawn as lines, and the 95% credible intervals as ribbons. **C.** Monthly time series of expected fire sizes for every level 3 ecoregion, faceted and colored by level 1 ecoregions sorted by mean humidity. Lines are posterior medians and ribbons are 95% credible intervals.

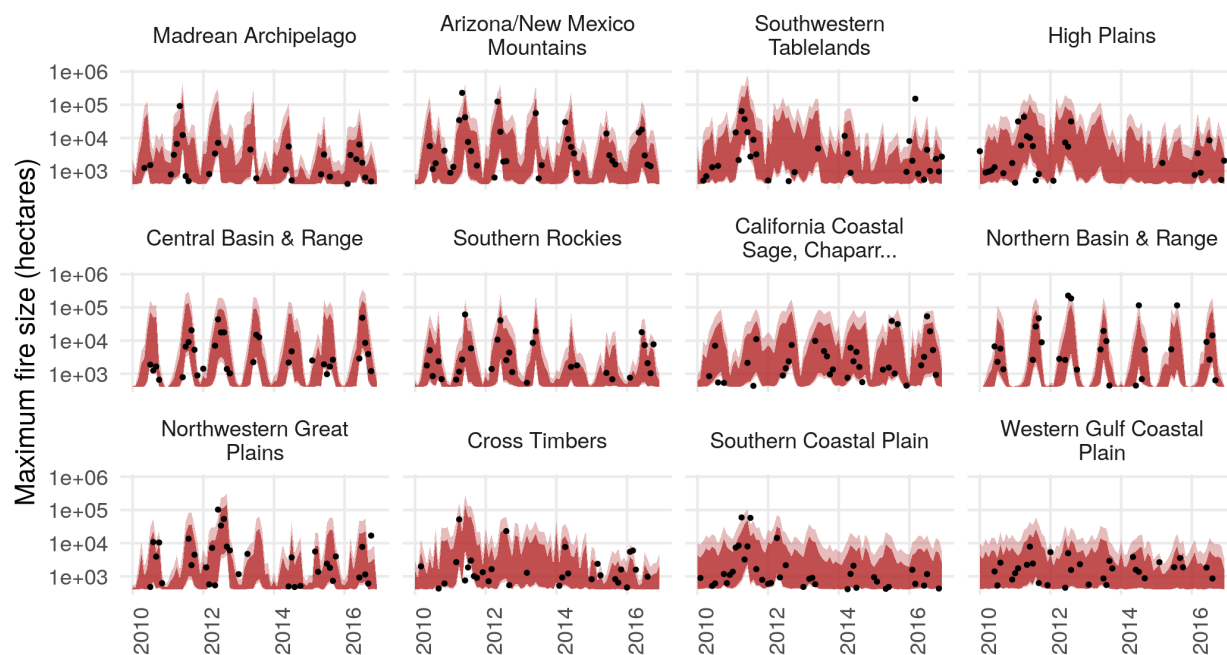


Figure 9. Posterior 99% (light red) and 95% (dark red) prediction intervals for the burned area of the largest fire event by month and level 3 ecoregion in the test set, shown for ecoregions with wildfires in more than 20 months. Empirical maxima are shown as black dots.

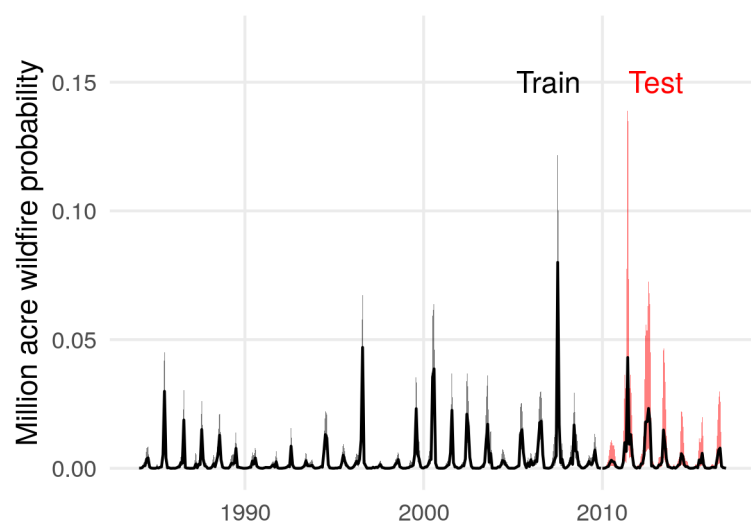


Figure 10. Estimated monthly posterior probabilities that one or more fire events exceed one million acres (404,686 hectares). The line represents the posterior median, and shaded region represents an 80% credible interval. The training period up to 2010 is shown in black, and the test period for which data were withheld during parameter estimation is shown in red.

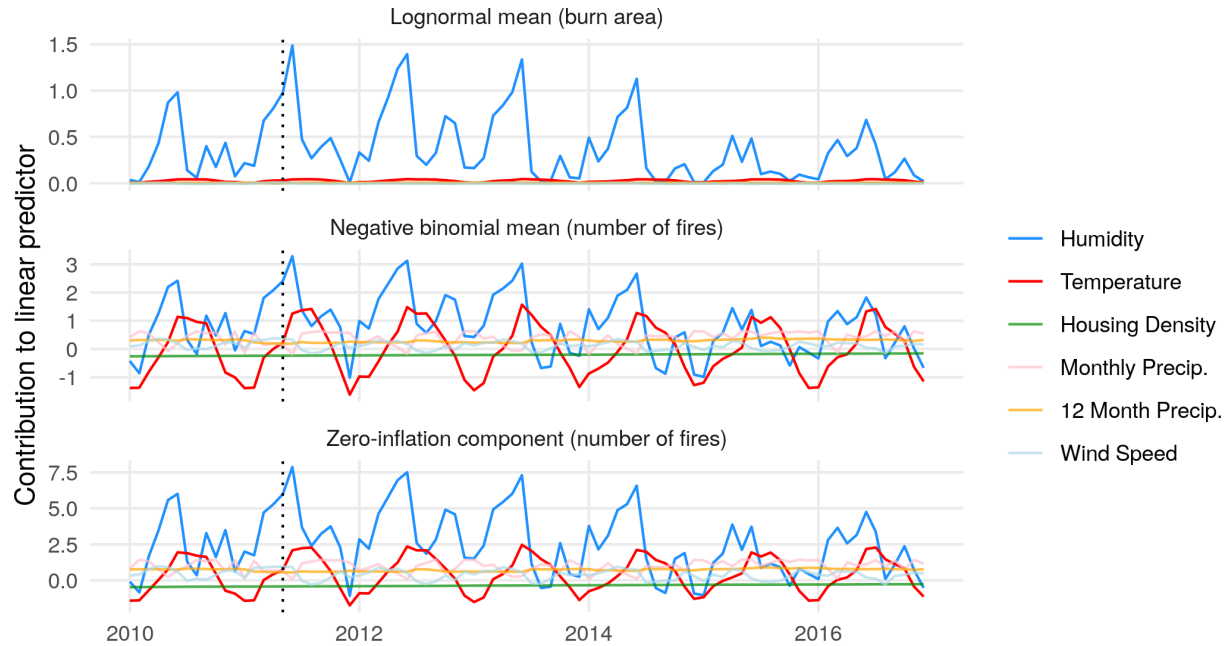


Figure 11. Posterior median contribution of each input variable to the linear predictor function of model components for the Arizona/New Mexico Mountains level 3 ecoregion from 2010-2016. A dotted vertical line marks May 2011, when the Wallow Fire ignited. Vertical positions of colored lines show contributions to the linear predictor function of each model component.

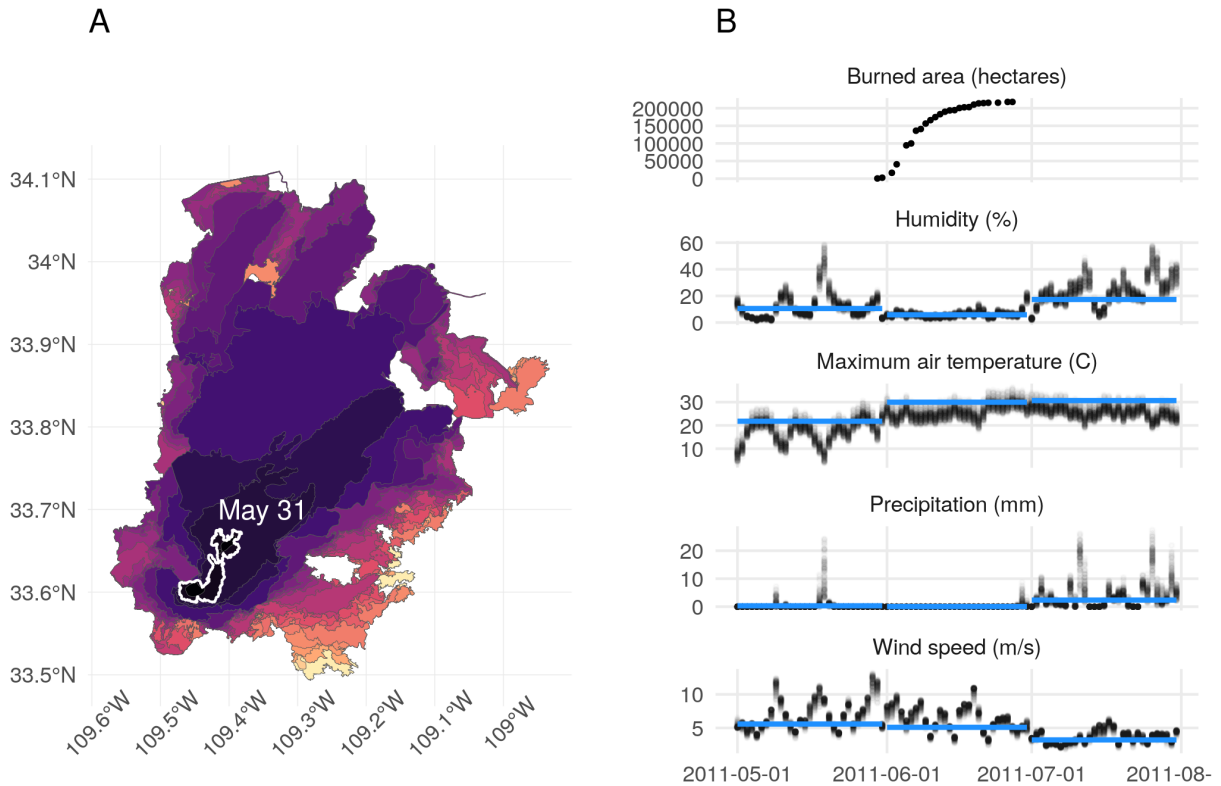


Figure 12. A. Progression of the Wallow Fire based on perimeter data collected from the GeoMAC database, spanning May 30, 2011 to June 27, 2011. The perimeter at the end of may is outlined in white, with brighter colors indicating later dates. B. Daily local meteorological conditions and monthly regional mean conditions for the Wallow Fire, along with the associated burned area over time. The blue line represents monthly averages of meteorological quantities computed over the entire Arizona/New Mexico Mountains ecoregion, and black points represent values extracted for "local" 4 km grid cells contained within the final burned area perimeter of the Wallow Fire.

782 Appendices

783 Prior specifications

784 Prior distributions were chosen to regularize coefficients on the distribution specific means
 785 $\beta^{(\mu)}$ and structural zero parameters $\beta^{(\pi)}$. We used a regularized horseshoe prior on these
 786 coefficients, which shrinks irrelevant coefficients towards zero, while regularizing nonzero
 787 coefficients (Piironen, Vehtari, and others 2017). For zero-inflated models, we used a multi-
 788 variate version of the regularized horseshoe (Peltola et al. 2014):

$$\begin{pmatrix} \beta_j^{(\mu)} \\ \beta_j^{(\pi)} \end{pmatrix} \sim \text{N} \left(\mathbf{0}, \begin{pmatrix} \tau_1^2 \tilde{\lambda}_{1,j}^2 & \rho \tau_1 \tau_2 \tilde{\lambda}_{1,j} \tilde{\lambda}_{2,j} \\ \rho \tau_1 \tau_2 \tilde{\lambda}_{1,j} \tilde{\lambda}_{2,j} & \tau_2^2 \tilde{\lambda}_{2,j}^2 \end{pmatrix} \right),$$

$$\tilde{\lambda}_{m,j}^2 = \frac{c_m^2 \lambda_j^2}{c_m^2 + \tau_m^2 \lambda_j^2},$$

789 for each response dimension $m = 1, 2$ and coefficient $j = 1, \dots, p$. Here ρ is a correlation
 790 parameter, τ_1 and τ_2 are global variance hyperparameters, c_1 and c_2 are hyperparameters
 791 that determine the amount of shrinkage on the largest coefficients, and λ_j is a local scale
 792 parameter drawn from a half-Cauchy distribution that control the amount of shrinkage
 793 applied to coefficient j (Piironen, Vehtari, and others 2017). With this prior specification,
 794 information can be shared across the two response dimensions through the correlation pa-
 795 rameter ρ , and/or through the local scale parameters λ_j . For count models without struc-
 796 tural zeros (the Poisson and negative binomial models), this multivariate prior simplifies to
 797 a univariate regularized horseshoe prior.

798 Spatiotemporal random effects were constructed using a temporally autoregressive, spa-
 799 tially intrinsically autoregressive formulation (Besag and Kooperberg 1995; Banerjee, Car-
 800 lin, and Gelfand 2014). Temporarily suppressing the superscript that indicates whether
 801 the effects are on μ or π , and denoting column t from an $S \times T$ Φ as ϕ_t we have:

$$\phi_{t=1} \sim \text{N}(\mathbf{0}, (\tau^{(\phi)}(\mathbf{D} - \mathbf{W}))^{-1})$$

$$\phi_t \sim N(\eta\phi_{t-1}, (\tau^{(\phi)}(\mathbf{D} - \mathbf{W}))^{-1}), \quad t = 2, \dots, T$$

802 where η is a temporal dependence parameter, $\tau^{(\phi)}$ is a precision parameter, \mathbf{D} is an $S \times S$
803 diagonal matrix with entries corresponding to the number of spatial neighbors for each
804 spatial unit, and \mathbf{W} is an $S \times S$ spatial adjacency matrix with nonzero elements only when
805 spatial unit i is a neighbor of spatial unit j ($w_{i,j} = 1$ if i is a neighbor of j , and $w_{i,j} = 0$
806 otherwise, including $w_{i,i} = 0$ for all i). $\tau^{(\phi)}$ is a precision parameter. We imposed a soft
807 identifiability constraint that places high prior mass near $\sum_{s=1}^S \phi_{t,s}^* = 0$ for all t .

808 We applied a univariate regularized horseshoe prior to all β coefficients in burned area
809 models (Piiironen, Vehtari, and others 2017):

$$\beta_j \sim N\left(0, \tau^2 \tilde{\lambda}_j^2\right), \quad \tilde{\lambda}_j^2 = \frac{c^2 \lambda_j^2}{c^2 + \tau^2 \lambda_j^2},$$

810 Spatiotemporal random effects were constructed in the same way as for the count models.

811 Joint distributions

812 Here we provide the unnormalized posterior densities for each model. Square brackets rep-
813 resent a probability mass or density function. Parameterizations for model likelihoods are
814 provided first, followed by the factorization of the joint distribution, with explicit priors.

815 Poisson wildfire count model

816 We used the following parameterization of the Poisson distribution:

$$[n|\mu] = \frac{\mu^n e^{-\mu}}{n!},$$

817 where μ is the mean and variance.

818 The unnormalized posterior density of this model is:

$$\begin{aligned} & [\boldsymbol{\beta}^{(\mu)}, \boldsymbol{\alpha}^{(\mu)}, \boldsymbol{\phi}, \sigma^{(\phi)}, \eta, \boldsymbol{\lambda}, c, \tau | \mathbf{N}] \propto \\ & \prod_{s=1}^S \prod_{t=1}^T [n_{s,t} | \boldsymbol{\beta}^{(\mu)}, \boldsymbol{\alpha}^{(\mu)}, \phi_{s,t}] \times \\ & [\boldsymbol{\phi}_1 | \sigma^{(\phi)}] \prod_{t=2}^T [\boldsymbol{\phi}_t | \boldsymbol{\phi}_{t-1}, \sigma^{(\phi)}, \eta] \times \\ & \prod_{j=1}^p [\beta_j^{(\mu)} | \lambda_j, c, \tau] [\lambda_j] \times \\ & [\sigma^{(\phi)}] [\eta] [c] [\tau] [\boldsymbol{\alpha}^{(\mu)}] \end{aligned}$$

$$\begin{aligned}
 &= \prod_{s=1}^S \prod_{t=1}^T \text{Poisson}(n_{s,t} | \exp(\alpha^{(\mu)} + \mathbf{X}_{(s,t)} \boldsymbol{\beta}^{(\mu)} + \phi_{s,t})) \times \\
 &\quad \text{Normal}(\boldsymbol{\phi}_1 | \mathbf{0}, ((\sigma^{(\phi)})^{-2}(\mathbf{D} - \mathbf{W}))^{-1}) \times \\
 &\quad \prod_{t=2}^T \text{Normal}(\boldsymbol{\phi}_t | \eta \boldsymbol{\phi}_{t-1}, ((\sigma^{(\phi)})^{-2}(\mathbf{D} - \mathbf{W}))^{-1}) \times \\
 &\quad \prod_{j=1}^p \text{Normal}\left(\beta_j^{(\mu)} | 0, \frac{\tau^2 c^2 \lambda_j^2}{c^2 + \tau^2 \lambda_j^2}\right) \times \text{Cauchy}^+(\lambda_j | 0, 1) \times \\
 &\text{Normal}^+(\sigma^{(\phi)} | 0, 1^2) \times \text{Beta}(\eta | 1, 1) \times \text{Inv-Gamma}(c^2 | 2.5, 10) \times \\
 &\quad \text{Normal}^+(\tau | 0, 5^2) \times \text{Normal}(\alpha^{(\mu)} | 0, 5^2).
 \end{aligned}$$

819 Negative binomial wildfire count model

820 We used the following parameterization of the negative binomial distribution:

$$[n|\mu, \delta] = \binom{n + \delta - 1}{n} \left(\frac{\mu}{\mu + \delta}\right)^n \left(\frac{\delta}{\mu + \delta}\right)^\delta,$$

821 where μ is the mean, and δ is a dispersion parameter.

822 The unnormalized posterior density of this model is:

$$\begin{aligned} & [\boldsymbol{\beta}^{(\mu)}, \boldsymbol{\alpha}^{(\mu)}, \boldsymbol{\phi}, \boldsymbol{\sigma}^{(\phi)}, \eta, \boldsymbol{\lambda}, c, \tau, \delta \mid \mathbf{N}] \propto \\ & \prod_{s=1}^S \prod_{t=1}^T [n_{s,t} | \boldsymbol{\beta}^{(\mu)}, \boldsymbol{\alpha}^{(\mu)}, \boldsymbol{\phi}_{s,t}, \delta] \times \\ & [\boldsymbol{\phi}_1 | \boldsymbol{\sigma}^{(\phi)}] \prod_{t=2}^T [\boldsymbol{\phi}_t | \boldsymbol{\phi}_{t-1}, \boldsymbol{\sigma}^{(\phi)}, \eta] \times \\ & \prod_{j=1}^p [\beta_j^{(\mu)} | \lambda_j, c, \tau] [\lambda_j] \times \\ & [\boldsymbol{\sigma}^{(\phi)}] [\eta] [c] [\tau] [\boldsymbol{\alpha}^{(\mu)}] [\delta] \end{aligned}$$

$$\begin{aligned} & = \prod_{s=1}^S \prod_{t=1}^T \text{Negative Binomial}(n_{s,t} | \exp(\boldsymbol{\alpha}^{(\mu)} + \mathbf{X}_{(s,t)} \boldsymbol{\beta}^{(\mu)} + \boldsymbol{\phi}_{s,t}), \delta) \times \\ & \text{Normal}(\boldsymbol{\phi}_1 | \mathbf{0}, ((\boldsymbol{\sigma}^{(\phi)})^{-2} (\mathbf{D} - \mathbf{W}))^{-1}) \times \\ & \prod_{t=2}^T \text{Normal}(\boldsymbol{\phi}_t | \eta \boldsymbol{\phi}_{t-1}, ((\boldsymbol{\sigma}^{(\phi)})^{-2} (\mathbf{D} - \mathbf{W}))^{-1}) \times \\ & \prod_{j=1}^p \text{Normal}\left(\beta_j^{(\mu)} | 0, \frac{\tau^2 c^2 \lambda_j^2}{c^2 + \tau^2 \lambda_j^2}\right) \times \text{Cauchy}^+(\lambda_j | 0, 1) \times \\ & \text{Normal}^+(\boldsymbol{\sigma}^{(\phi)} | 0, 1^2) \times \text{Beta}(\eta | 1, 1) \times \text{Inv-Gamma}(c^2 | 2.5, 10) \times \\ & \text{Normal}^+(\tau | 0, 5^2) \times \text{Normal}(\boldsymbol{\alpha}^{(\mu)} | 0, 5^2) \times \text{Normal}^+(\delta | 0, 5^2). \end{aligned}$$

823 **Zero-inflated Poisson wildfire count model**

824 We used the following parameterization of the zero-inflated Poisson distribution:

$$[n|\mu, \pi] = I_{n=0}(1 - \pi + \pi e^{-\mu}) + I_{n>0}\pi \frac{\mu^n e^{-\mu}}{n!},$$

825 where μ is the Poisson mean, and $1 - \pi$ is the probability of an extra zero.

826 The unnormalized posterior density of this model is:

$$\begin{aligned} & [\boldsymbol{\beta}^{(\mu)}, \alpha^{(\mu)}, \boldsymbol{\beta}^{(\pi)}, \alpha^{(\pi)}, \boldsymbol{\phi}^{(\mu)}, \sigma^{(\phi, \mu)}, \eta^{(\mu)}, \boldsymbol{\phi}^{(\pi)}, \sigma^{(\phi, \pi)}, \eta^{(\pi)}, \boldsymbol{\lambda}, c, \tau, \rho | \mathbf{N}] \propto \\ & \prod_{s=1}^S \prod_{t=1}^T [n_{s,t} | \boldsymbol{\beta}^{(\mu)}, \alpha^{(\mu)}, \boldsymbol{\beta}^{(\pi)}, \alpha^{(\pi)}, \phi_{s,t}^{(\mu)}, \phi_{s,t}^{(\pi)}] \times \\ & [\phi_1^{(\mu)} | \sigma^{(\phi, \mu)}] \prod_{t=2}^T [\phi_t^{(\mu)} | \phi_{t-1}^{(\mu)}, \sigma^{(\phi, \mu)}, \eta^{(\mu)}] \times \\ & [\phi_1^{(\pi)} | \sigma^{(\phi, \pi)}] \prod_{t=2}^T [\phi_t^{(\pi)} | \phi_{t-1}^{(\pi)}, \sigma^{(\phi, \pi)}, \eta^{(\pi)}] \times \\ & \prod_{j=1}^p [\beta_j^{(\mu)}, \beta_j^{(\pi)} | \lambda_j, c, \tau, \rho] [\lambda_j] \times \\ & [\sigma^{(\phi, \mu)}] [\sigma^{(\phi, \pi)}] [\eta^{(\mu)}] [\eta^{(\pi)}] [\alpha^{(\mu)}] [\alpha^{(\pi)}] [\rho] \prod_{m=1}^2 [c_m] [\tau_m] \end{aligned}$$

$$\begin{aligned}
 &= \prod_{s=1}^S \prod_{t=1}^T \text{ZIP}(n_{s,t} | e^{\alpha^{(\mu)} + \mathbf{X}_{(s,t)} \boldsymbol{\beta}^{(\mu)} + \phi_{s,t}^{(\mu)}}, \text{logit}^{-1}(\alpha^{(\pi)} + \mathbf{X}_{(s,t)} \boldsymbol{\beta}^{(\pi)} + \phi_{s,t}^{(\pi)})) \times \\
 &\quad \text{Normal}(\boldsymbol{\phi}_1^{(\mu)} | \mathbf{0}, ((\sigma^{(\phi, \mu)})^{-2}(\mathbf{D} - \mathbf{W}))^{-1}) \times \\
 &\quad \prod_{t=2}^T \text{Normal}(\boldsymbol{\phi}_t^{(\mu)} | \eta^{(\mu)} \boldsymbol{\phi}_{t-1}^{(\mu)}, ((\sigma^{(\phi, \mu)})^{-2}(\mathbf{D} - \mathbf{W}))^{-1}) \times \\
 &\quad \text{Normal}(\boldsymbol{\phi}_1^{(\pi)} | \mathbf{0}, ((\sigma^{(\phi, \pi)})^{-2}(\mathbf{D} - \mathbf{W}))^{-1}) \times \\
 &\quad \prod_{t=2}^T \text{Normal}(\boldsymbol{\phi}_t^{(\pi)} | \eta^{(\pi)} \boldsymbol{\phi}_{t-1}^{(\pi)}, ((\sigma^{(\phi, \pi)})^{-2}(\mathbf{D} - \mathbf{W}))^{-1}) \times \\
 &\quad \prod_{j=1}^p \text{N} \left(\begin{pmatrix} \beta_j^{(\mu)} \\ \beta_j^{(\pi)} \end{pmatrix} \middle| \mathbf{0}, \begin{pmatrix} \tau_1^2 \frac{c_1^2 \lambda_j^2}{c_1^2 + \tau_1^2 \lambda_j^2} & \rho \tau_1 \tau_2 \sqrt{\frac{c_1^2 \lambda_j^2}{c_1^2 + \tau_1^2 \lambda_j^2}} \sqrt{\frac{c_2^2 \lambda_j^2}{c_2^2 + \tau_2^2 \lambda_j^2}} \\ \rho \tau_1 \tau_2 \sqrt{\frac{c_1^2 \lambda_j^2}{c_1^2 + \tau_1^2 \lambda_j^2}} \sqrt{\frac{c_2^2 \lambda_j^2}{c_2^2 + \tau_2^2 \lambda_j^2}} & \tau_2^2 \frac{c_2^2 \lambda_j^2}{c_2^2 + \tau_2^2 \lambda_j^2} \end{pmatrix} \right) \times \\
 &\quad \prod_{j=1}^p \text{Cauchy}^+(\lambda_j | 0, 1) \times \\
 &\quad \text{Normal}^+(\sigma^{(\phi, \mu)} | 0, 1^2) \times \text{Normal}^+(\sigma^{(\phi, \pi)} | 0, 1^2) \times \\
 &\quad \text{Beta}(\eta^{(\mu)} | 1, 1) \times \text{Beta}(\eta^{(\pi)} | 1, 1) \times \\
 &\quad \text{Normal}(\alpha^{(\mu)} | 0, 5^2) \times \text{Normal}(\alpha^{(\pi)} | 0, 5^2) \times \text{LKJ}(\rho | 3) \times \\
 &\quad \prod_{m=1}^2 \text{Inv-Gamma}(c_m^2 | 2.5, 10) \times \text{Normal}^+(\tau_m | 0, 5^2).
 \end{aligned}$$

827 **Zero-inflated negative binomial wildfire count model**

828 We used the following parameterization of the zero-inflated negative binomial distribution:

$$[n|\mu, \delta, \pi] = I_{n=0}(1 - \pi + \pi\left(\frac{\delta}{\mu + \delta}\right)^\delta) + I_{n>0}\binom{n + \delta - 1}{n}\left(\frac{\mu}{\mu + \delta}\right)^n\left(\frac{\delta}{\mu + \delta}\right)^\delta,$$

829 where μ is the negative binomial mean, δ is the negative binomial dispersion, and , and

830 $1 - \pi$ is the probability of an extra zero.

831 The unnormalized posterior density of this model is:

$$\begin{aligned} & [\boldsymbol{\beta}^{(\mu)}, \alpha^{(\mu)}, \boldsymbol{\beta}^{(\pi)}, \alpha^{(\pi)}, \boldsymbol{\phi}^{(\mu)}, \sigma^{(\phi, \mu)}, \eta^{(\mu)}, \boldsymbol{\phi}^{(\pi)}, \sigma^{(\phi, \pi)}, \eta^{(\pi)}, \boldsymbol{\lambda}, c, \tau, \rho, \delta | \mathbf{N}] \propto \\ & \prod_{s=1}^S \prod_{t=1}^T [n_{s,t} | \boldsymbol{\beta}^{(\mu)}, \alpha^{(\mu)}, \boldsymbol{\beta}^{(\pi)}, \alpha^{(\pi)}, \phi_{s,t}^{(\mu)}, \phi_{s,t}^{(\pi)}, \delta] \times \\ & [\phi_1^{(\mu)} | \sigma^{(\phi, \mu)}] \prod_{t=2}^T [\phi_t^{(\mu)} | \phi_{t-1}^{(\mu)}, \sigma^{(\phi, \mu)}, \eta^{(\mu)}] \times \\ & [\phi_1^{(\pi)} | \sigma^{(\phi, \pi)}] \prod_{t=2}^T [\phi_t^{(\pi)} | \phi_{t-1}^{(\pi)}, \sigma^{(\phi, \pi)}, \eta^{(\pi)}] \times \\ & \prod_{j=1}^p [\beta_j^{(\mu)}, \beta_j^{(\pi)} | \lambda_j, c, \tau, \rho] [\lambda_j] \times \\ & [\sigma^{(\phi, \mu)}][\sigma^{(\phi, \pi)}][\eta^{(\mu)}][\eta^{(\pi)}][\alpha^{(\mu)}][\alpha^{(\pi)}][\rho][\delta] \prod_{m=1}^2 [c_m][\tau_m]. \end{aligned}$$

$$\begin{aligned}
 &= \prod_{s=1}^S \prod_{t=1}^T \text{ZINB}(n_{s,t} | e^{\alpha^{(\mu)} + \mathbf{X}_{(s,t)} \boldsymbol{\beta}^{(\mu)} + \phi_{s,t}^{(\mu)}}, \delta, \text{logit}^{-1}(\alpha^{(\pi)} + \mathbf{X}_{(s,t)} \boldsymbol{\beta}^{(\pi)} + \phi_{s,t}^{(\pi)})) \times \\
 &\quad \text{Normal}(\boldsymbol{\phi}_1^{(\mu)} | \mathbf{0}, ((\sigma^{(\phi, \mu)})^{-2}(\mathbf{D} - \mathbf{W}))^{-1}) \times \\
 &\quad \prod_{t=2}^T \text{Normal}(\boldsymbol{\phi}_t^{(\mu)} | \boldsymbol{\eta}^{(\mu)} \boldsymbol{\phi}_{t-1}^{(\mu)}, ((\sigma^{(\phi, \mu)})^{-2}(\mathbf{D} - \mathbf{W}))^{-1}) \times \\
 &\quad \text{Normal}(\boldsymbol{\phi}_1^{(\pi)} | \mathbf{0}, ((\sigma^{(\phi, \pi)})^{-2}(\mathbf{D} - \mathbf{W}))^{-1}) \times \\
 &\quad \prod_{t=2}^T \text{Normal}(\boldsymbol{\phi}_t^{(\pi)} | \boldsymbol{\eta}^{(\pi)} \boldsymbol{\phi}_{t-1}^{(\pi)}, ((\sigma^{(\phi, \pi)})^{-2}(\mathbf{D} - \mathbf{W}))^{-1}) \times \\
 &\quad \prod_{j=1}^p \text{N} \left(\begin{pmatrix} \beta_j^{(\mu)} \\ \beta_j^{(\pi)} \end{pmatrix} \middle| \mathbf{0}, \begin{pmatrix} \tau_1^2 \frac{c_1^2 \lambda_j^2}{c_1^2 + \tau_1^2 \lambda_j^2} & \rho \tau_1 \tau_2 \sqrt{\frac{c_1^2 \lambda_j^2}{c_1^2 + \tau_1^2 \lambda_j^2}} \sqrt{\frac{c_2^2 \lambda_j^2}{c_2^2 + \tau_2^2 \lambda_j^2}} \\ \rho \tau_1 \tau_2 \sqrt{\frac{c_1^2 \lambda_j^2}{c_1^2 + \tau_1^2 \lambda_j^2}} \sqrt{\frac{c_2^2 \lambda_j^2}{c_2^2 + \tau_2^2 \lambda_j^2}} & \tau_2^2 \frac{c_2^2 \lambda_j^2}{c_2^2 + \tau_2^2 \lambda_j^2} \end{pmatrix} \right) \times \\
 &\quad \prod_{j=1}^p \text{Cauchy}^+(\lambda_j | 0, 1) \times \\
 &\quad \text{Normal}^+(\sigma^{(\phi, \mu)} | 0, 1^2) \times \text{Normal}^+(\sigma^{(\phi, \pi)} | 0, 1^2) \times \\
 &\quad \text{Beta}(\boldsymbol{\eta}^{(\mu)} | 1, 1) \times \text{Beta}(\boldsymbol{\eta}^{(\pi)} | 1, 1) \times \\
 &\quad \text{Normal}(\alpha^{(\mu)} | 0, 5^2) \times \text{Normal}(\alpha^{(\pi)} | 0, 5^2) \times \text{LKJ}(\rho | 3) \times \text{Normal}^+(\delta | 0, 5^2) \times \\
 &\quad \prod_{m=1}^2 \text{Inv-Gamma}(c_m^2 | 2.5, 10) \times \text{Normal}^+(\tau_m | 0, 5^2).
 \end{aligned}$$

832 **Generalized Pareto/Lomax burned area model**

833 We used the following parameterization of the GPD/Lomax distribution:

$$[y|\sigma, \kappa] = \frac{1}{\sigma} \left(\frac{\kappa y}{\sigma} + 1 \right)^{-(\kappa+1)\kappa^{-1}},$$

834 where κ is a shape parameter and σ is a scale parameter.

835 The unnormalized posterior density of this model is:

$$\begin{aligned} & [\boldsymbol{\beta}, \alpha, \boldsymbol{\phi}, \sigma^{(\phi)}, \eta, \kappa^{(L)}, \boldsymbol{\lambda}, c, \tau | \mathbf{y}] \propto \\ & \prod_{i=1}^{n_{\text{tot}}} [y_i | \boldsymbol{\beta}, \alpha, \phi_{s_i, t_i}, \kappa^{(L)}] \times \\ & [\boldsymbol{\phi}_1 | \sigma^{(\phi)}] \prod_{t=2}^T [\boldsymbol{\phi}_t | \boldsymbol{\phi}_{t-1}, \sigma^{(\phi)}, \eta] \times \\ & \prod_{j=1}^p [\beta_j | \lambda_j, c, \tau] [\lambda_j] \times \\ & [\alpha][c][\tau][\kappa^{(L)}][\eta][\sigma^{(\phi)}] \\ & = \prod_{i=1}^{n_{\text{tot}}} \text{Lomax}(y_i | \kappa^{(L)}, e^{\alpha + \mathbf{X}_{(s_i, t_i)} \boldsymbol{\beta} + \phi_{s_i, t_i}}) \times \\ & \text{Normal}(\boldsymbol{\phi}_1 | \mathbf{0}, ((\sigma^{(\phi)})^{-2}(\mathbf{D} - \mathbf{W}))^{-1}) \times \\ & \prod_{t=2}^T \text{Normal}(\boldsymbol{\phi}_t | \eta \boldsymbol{\phi}_{t-1}, ((\sigma^{(\phi)})^{-2}(\mathbf{D} - \mathbf{W}))^{-1}) \times \\ & \prod_{j=1}^p \text{Normal}\left(\beta_j | 0, \frac{\tau^2 c^2 \lambda_j^2}{c^2 + \tau^2 \lambda_j^2}\right) \times \text{Cauchy}^+(\lambda_j | 0, 1) \times \\ & \text{Normal}(\alpha | 0, 5^2) \times \text{Inv-Gamma}(c^2 | 2.5, 10) \times \text{Normal}^+(\tau | 0, 5^2) \\ & \text{Normal}^+(\kappa^{(L)} | 0, 5^2) \times \text{Beta}(\eta | 1, 1) \times \text{Normal}^+(\sigma^{(\phi)} | 0, 1^2). \end{aligned}$$

836 **Tapered Pareto burned area model**

837 We used the following parameterization of the tapered Pareto distribution:

$$[y|\kappa, \nu] = \left(\frac{\kappa}{y} + \frac{1}{\nu}\right) \exp(-x/\nu),$$

838 where κ is a shape parameter and ν a taper parameter.

839 The unnormalized posterior density of this model is:

$$\begin{aligned} & [\boldsymbol{\beta}, \alpha, \boldsymbol{\phi}, \sigma^{(\phi)}, \eta, \nu, \boldsymbol{\lambda}, c, \tau | \mathbf{y}] \propto \\ & \prod_{i=1}^{n_{\text{tot}}} [y_i | \boldsymbol{\beta}, \alpha, \phi_{s_i, t_i}, \nu] \times \\ & [\boldsymbol{\phi}_1 | \sigma^{(\phi)}] \prod_{t=2}^T [\boldsymbol{\phi}_t | \boldsymbol{\phi}_{t-1}, \sigma^{(\phi)}, \eta] \times \\ & \prod_{j=1}^p [\beta_j | \lambda_j, c, \tau] [\lambda_j] \times \\ & [\alpha] [c] [\tau] [\nu] [\eta] [\sigma^{(\phi)}] \\ & = \prod_{i=1}^{n_{\text{tot}}} \text{Tapered Pareto}(y_i | e^{\alpha + \mathbf{X}_{(s_i, t_i)} \boldsymbol{\beta} + \phi_{s_i, t_i}}, \nu) \times \\ & \quad \text{Normal}(\boldsymbol{\phi}_1 | \mathbf{0}, ((\sigma^{(\phi)})^{-2} (\mathbf{D} - \mathbf{W}))^{-1}) \times \\ & \quad \prod_{t=2}^T \text{Normal}(\boldsymbol{\phi}_t | \eta \boldsymbol{\phi}_{t-1}, ((\sigma^{(\phi)})^{-2} (\mathbf{D} - \mathbf{W}))^{-1}) \times \\ & \quad \prod_{j=1}^p \text{Normal}\left(\beta_j | 0, \frac{\tau^2 c^2 \lambda_j^2}{c^2 + \tau^2 \lambda_j^2}\right) \times \text{Cauchy}^+(\lambda_j | 0, 1) \times \\ & \quad \text{Normal}(\alpha | 0, 5^2) \times \text{Inv-Gamma}(c^2 | 2.5, 10) \times \text{Normal}^+(\tau | 0, 5^2) \times \\ & \quad \text{Cauchy}^+(\nu | 0, 1) \times \text{Beta}(\eta | 1, 1) \times \text{Normal}^+(\sigma^{(\phi)} | 0, 1^2). \end{aligned}$$

840 **Lognormal burned area model**

841 We used the following parameterization of the lognormal distribution:

$$[y|\mu, \sigma] = \frac{1}{y} \frac{1}{\sigma\sqrt{2\pi}} \exp\left(-\frac{(\log(y) - \mu)^2}{2\sigma^2}\right),$$

842 where μ and σ are location and scale parameters, respectively.

843 The unnormalized posterior density of this model is:

$$\begin{aligned} [\boldsymbol{\beta}, \alpha, \boldsymbol{\phi}, \sigma^{(\phi)}, \eta, \sigma, \boldsymbol{\lambda}, c, \tau | \mathbf{y}] &\propto \\ &\prod_{i=1}^{n_{\text{tot}}} [y_i | \beta, \alpha, \phi_{s_i, t_i}, \sigma] \times \\ &[\boldsymbol{\phi}_1 | \sigma^{(\phi)}] \prod_{t=2}^T [\boldsymbol{\phi}_t | \boldsymbol{\phi}_{t-1}, \sigma^{(\phi)}, \eta] \times \\ &\prod_{j=1}^p [\beta_j | \lambda_j, c, \tau] [\lambda_j] \times \\ &[\alpha][c][\tau][\sigma][\eta][\sigma^{(\phi)}] \\ &= \prod_{i=1}^{n_{\text{tot}}} \text{Lognormal}(y_i | \alpha + \mathbf{X}_{(s_i, t_i)} \boldsymbol{\beta} + \phi_{s_i, t_i}, \sigma) \times \\ &\quad \text{Normal}(\boldsymbol{\phi}_1 | \mathbf{0}, ((\sigma^{(\phi)})^{-2}(\mathbf{D} - \mathbf{W}))^{-1}) \times \\ &\quad \prod_{t=2}^T \text{Normal}(\boldsymbol{\phi}_t | \eta \boldsymbol{\phi}_{t-1}, ((\sigma^{(\phi)})^{-2}(\mathbf{D} - \mathbf{W}))^{-1}) \times \\ &\quad \prod_{j=1}^p \text{Normal}\left(\beta_j | 0, \frac{\tau^2 c^2 \lambda_j^2}{c^2 + \tau^2 \lambda_j^2}\right) \times \text{Cauchy}^+(\lambda_j | 0, 1) \times \\ &\quad \text{Normal}(\alpha | 0, 5^2) \times \text{Inv-Gamma}(c^2 | 2.5, 10) \times \text{Normal}^+(\tau | 0, 5^2) \times \\ &\quad \text{Normal}^+(\sigma | 0, 5^2) \times \text{Beta}(\eta | 1, 1) \times \text{Normal}^+(\sigma^{(\phi)} | 0, 1^2). \end{aligned}$$

844 **Gamma burned area model**

845 We used the following parameterization of the gamma distribution:

$$[y|\kappa, \sigma] = \frac{1}{\Gamma(\kappa)\sigma^\kappa} y^{\kappa-1} \exp(-y/\sigma),$$

846 where κ is a shape parameter and σ a scale parameter.

847 The unnormalized posterior density of this model is:

$$\begin{aligned} & [\boldsymbol{\beta}, \alpha, \boldsymbol{\phi}, \sigma^{(\phi)}, \eta, \kappa, \boldsymbol{\lambda}, c, \tau | \mathbf{y}] \propto \\ & \prod_{i=1}^{n_{\text{tot}}} [y_i | \beta, \alpha, \phi_{s_i, t_i}, \kappa] \times \\ & [\boldsymbol{\phi}_1 | \sigma^{(\phi)}] \prod_{t=2}^T [\boldsymbol{\phi}_t | \boldsymbol{\phi}_{t-1}, \sigma^{(\phi)}, \eta] \times \\ & \prod_{j=1}^p [\beta_j | \lambda_j, c, \tau] [\lambda_j] \times \\ & [\alpha] [c] [\tau] [\kappa] [\eta] [\sigma^{(\phi)}] \\ & = \prod_{i=1}^{n_{\text{tot}}} \text{Gamma}(y_i | \kappa, \kappa / \exp(\alpha + \mathbf{X}_{(s_i, t_i)} \boldsymbol{\beta} + \phi_{s_i, t_i})) \times \\ & \quad \text{Normal}(\boldsymbol{\phi}_1 | \mathbf{0}, ((\sigma^{(\phi)})^{-2} (\mathbf{D} - \mathbf{W}))^{-1}) \times \\ & \quad \prod_{t=2}^T \text{Normal}(\boldsymbol{\phi}_t | \eta \boldsymbol{\phi}_{t-1}, ((\sigma^{(\phi)})^{-2} (\mathbf{D} - \mathbf{W}))^{-1}) \times \\ & \quad \prod_{j=1}^p \text{Normal}\left(\beta_j | 0, \frac{\tau^2 c^2 \lambda_j^2}{c^2 + \tau^2 \lambda_j^2}\right) \times \text{Cauchy}^+(\lambda_j | 0, 1) \times \\ & \quad \text{Normal}(\alpha | 0, 5^2) \times \text{Inv-Gamma}(c^2 | 2.5, 10) \times \text{Normal}^+(\tau | 0, 5^2) \times \\ & \quad \text{Normal}^+(\kappa | 0, 5^2) \times \text{Beta}(\eta | 1, 1) \times \text{Normal}^+(\sigma^{(\phi)} | 0, 1^2). \end{aligned}$$

848 **Weibull burned area model**

849 We used the following parameterization of the Weibull distribution:

$$[y|\kappa, \sigma] = \frac{\kappa}{\sigma} \left(\frac{y}{\sigma}\right)^{\kappa-1} \exp\left(-\left(\frac{y}{\sigma}\right)^\kappa\right),$$

850 where κ is a shape parameter and σ is a scale parameter.

851 The unnormalized posterior density of this model is:

$$\begin{aligned} [\boldsymbol{\beta}, \alpha, \boldsymbol{\phi}, \sigma^{(\phi)}, \eta, \kappa, \lambda, c, \tau | \mathbf{y}] &\propto \\ &\prod_{i=1}^{n_{\text{tot}}} [y_i | \beta, \alpha, \phi_{s_i, t_i}, \kappa] \times \\ &[\boldsymbol{\phi}_1 | \sigma^{(\phi)}] \prod_{t=2}^T [\boldsymbol{\phi}_t | \boldsymbol{\phi}_{t-1}, \sigma^{(\phi)}, \eta] \times \\ &\prod_{j=1}^p [\beta_j | \lambda_j, c, \tau] [\lambda_j] \times \\ &[\alpha] [c] [\tau] [\kappa] [\eta] [\sigma^{(\phi)}] \\ &= \prod_{i=1}^{n_{\text{tot}}} \text{Weibull}(y_i | \kappa, \exp(\alpha + \mathbf{X}_{(s_i, t_i)} \boldsymbol{\beta} + \phi_{s_i, t_i})) \times \\ &\quad \text{Normal}(\boldsymbol{\phi}_1 | \mathbf{0}, ((\sigma^{(\phi)})^{-2} (\mathbf{D} - \mathbf{W}))^{-1}) \times \\ &\quad \prod_{t=2}^T \text{Normal}(\boldsymbol{\phi}_t | \eta \boldsymbol{\phi}_{t-1}, ((\sigma^{(\phi)})^{-2} (\mathbf{D} - \mathbf{W}))^{-1}) \times \\ &\quad \prod_{j=1}^p \text{Normal}\left(\beta_j | 0, \frac{\tau^2 c^2 \lambda_j^2}{c^2 + \tau^2 \lambda_j^2}\right) \times \text{Cauchy}^+(\lambda_j | 0, 1) \times \\ &\quad \text{Normal}(\alpha | 0, 5^2) \times \text{Inv-Gamma}(c^2 | 2.5, 10) \times \text{Normal}^+(\tau | 0, 5^2) \times \\ &\quad \text{Normal}^+(\kappa | 0, 5^2) \times \text{Beta}(\eta | 1, 1) \times \text{Normal}^+(\sigma^{(\phi)} | 0, 1^2). \end{aligned}$$